SKB

TECHNICAL REPORT 87-14

Combined interpretation of geophysical, geological, hydrological and radar investigations in the boreholes ST1 and ST2 at the Saltsjötunnel

Jan-Erik Andersson
Per Andersson
Seje Carlsten
Lars Falk
Olle Olsson
Allan Stråhle

Swedish Geological Co, Uppsala
June 1987

SVENSK KÄRNBRÄNSLEHANTERING AB
SWEDISH NUCLEAR FUEL AND WASTE MANAGEMENT CO

BOX 5864 S-102 48 STOCKHOLM
TEL 08-665 28 00 TELEX 13108-SKB

COMBINED INTERPRETATION OF GEOPHYSICAL, GEOLOGICAL, HYDROLOGICAL AND RADAR INVESTIGATIONS IN THE BOREHOLES ST1 AND ST2 AT THE SALTSJÖTUNNEL

Jan-Erik Andersson
Per Andersson
Seje Carlsten
Lars Falk
Olle Olsson
Allan Stråhle

Swedish Geological Co, Uppsala

1987-06-30

SWEDISH GEOLOGICAL Co.
Engineering geology
Uppsala, Sweden

REPORT
ID-nr:87 365
Date:1987-06-30

COMBINED INTERPRETATION OF GEOPHYSICAL, GEOLOGICAL, HYDROLOGICAL AND RADAR INVESTIGATIONS IN THE BOREHOLES ST1 AND ST2 AT THE SALTSJÖTUNNEL

Jan-Erik Andersson
Per Andersson
Seje Carlsten
Lars Falk
Olle Olsson
Allan Stråhle

Page

ABSTRACT

CONTENTS

SUMMARY

1	INTRODUCTION	1
2	DESCRIPTION OF THE SITE	4
3	INVESTIGATION PROGRAM	7
3.1	Geological core mapping	7
3.1.1	Drill core mapping	7
3.1.2	Equipment for geological core mapping	11
3.2	Geophysical borehole logging	12
3.2.1	Logging program and instruments	12
3.3	Hydraulic singlehole tests	17
3.3.1	Test program and interpretation	17
3.3.2	Equipment for hydraulic tests	19
3.4	Borehole radar investigation	22
3.4.1	Radar measurement	22
3.4.2	Equipment for borehole radar investigation	24
4	GENERAL RESULTS OF THE BOREHOLE INVESTIGATIONS	28
4.1	Geological core mapping	29
4.2	Geophysical borehole logging	34
4.3	Hydraulic singlehole tests	40
4.4	Borehole radar investigation	43

5	COMBINED INTERPRETATION	58
5.1	Major structures interpreted by borehole radar measurements compared to geological, geophysical and hydraulic results	58
5.2	Geophysical, geological and hydraulic data compared with radar interpreted structures	60
5.3	Results of combined interpretation	64
6	CONCLUSIONS	69
7	DISCUSSION	70
	REFERENCES	73
	APPENDIX 1 : Technical data for boreholes ST1 and ST2	

ABSTRACT

Radar measurements have been used to produce a model of the geological structures along a section of the Saltsjötunnel. The model was arrived at without access to any other geological, geophysical or hydrological data except a topographic map of the site. The radar model has then been compared to results from core mapping, geophysical logging and hydraulic borehole measurements. All available data have been put together to check the validity of the radar model and then to revise it in order to obtain an improved model of the site.

The model produced by the radar results have in general been in agreement with the result of the other borehole investigations. The combined interpretation reveals two sets: the first set is adjoined with lithological variations in the bedrock striking roughly N-S with a more or less vertical dip. The second subhorizontal set which constitute the most prominent fracture zones is striking NW with a dip 35^{o} towards NE. The combined interpretation resulted in a model comprising three dominating subhorizontal zones. The three subhorizontal zones are interpreted to be the most dominating fracture zones within the investigated area.

1 INTRODUCTION

The borehole radar technique has been developed to its present status by a group at the Swedish Geological Co. funded by the International Stripa Project and SKB. The technique was developed with the objective to map the extension and character of fracture zones. The radar technique has previously been applied within the SKB Research and Development Program at the investigation sites Finnsjön, Ävrö, and Klipperås. The results from these sites have generally been of high quality and have demonstrated the capability of radar to describe the geometry of geological features such as dykes and fracture zones. The investigation range in single hole reflection mode has varied from 40 m (Finnsjön) to 120 m (Klipperås) depending on the electrical properties of the rock.

In Solna STOSEB (the energy supply company of Greater Stockholm) has let built a heating plant where the heat from purified waste water is extracted. The waste water is taken from the Bromma purifying plant. Instead of returning the water back to Bromma after the extraction, STOSEB and the Waterworks of Stockholm decided to transfer the purified water directly to Saltsjön through a tunnel. The tunnel for this purpose is intended to be excavated at a length of 7.6 km in crystalline rock. The investigation carried out in this report is a part of a larger research work connected to the excavation and construction of the Saltsjötunnel.

The borehole radar technique is relatively new and there is a need of results and interpretational experience from different geological environments. The excavation of the Saltsjötunnel was considered to provide a good possibility for testing the predictive capabilites of the radar method in connection to underground construction work. Radar investigations were performed and evaluated without access to any other geological information (Carlsten et al, 1987). Then followed a combined evaluation of all borehole investigation which is presented in this report. These results will later be compared with data collected in the tunnel.

Two holes were drilled from a position above the planned extension of

the tunnel. The holes are drilled from essentially the same point at the ground surface and both have a dip of 60^{o} but are drilled in opposite directions. The holes thus outline an equilateral triangle with its plane parallel to the tunnel direction. This borehole layout was considered to give a good possibility for describing the geological structures in the vicinity of the tunnel for a length of about 70 m. The holes were drilled and radar measurements performed prior to any other geological or geophysical investigation. In this way it is possible to get an idea of what an interpretation of radar results can give which is unbiased by any other geological or geophysical results. This radar interpretation is compared with results obtained from the other investigations in the holes which comprises geological core mapping, geophysical logging, and hydraulic testing. The excavation of the tunnel will later provide a means for comparing the borehole results with observations and measurements made in the tunnel.

The radar investigation gives a geometrical model of the geological structures at the site. Estimates are also obtained of the physical properties and the geological character of the identified structures. The comparison, performed in this report, of the radar results with other borehole investigations will give a measure on the reliability of the radar model in various aspects such as positional accuracy and character of identified structures.

The borehole radar technique has for this investigation been applied in three different modes; singlehole reflection, crosshole reflection and crosshole tomography. Singlehole reflection measurements have been made in the holes ST1 and ST2 with two different center frequencies, namely 22 and 60 MHz. Crosshole measurements were also performed at these two frequencies. Note that the data for crosshole reflection and crosshole tomography are obtained from the same measurement.

The hydraulic singlehole tests were carried out as short-time constant-pressure injection tests. A few borehole intervals were selected for detailed transient testing. A transient single-packer test of the entire borehole length was performed in both boreholes. The hydraulic singlehole tests were performed after completion of radar measurements.

The geophysical singlehole investigation performed in both boreholes comprised the following logs; natural gamma, single point resistance, normal resistivity, neutron, temperature, and borehole fluid resistivity. The temperature gradient and salinity of the borehole fluid were calculated from the temperature log and the temperature/fluid resistivity logs, respectively. The geophysical borehole measurements were performed after completion of the hydraulic measurements.

The geological core mapping was performed with a microcomputer-based core mapping system. The core was mapped with emphasis put on rock type, fractures and fracture minerals. The core mapping was performed at about the same time as the geophysical investigation.

This report presents the investigation program, general results and a combined interpretation of the data obtained from the four independently performed investigations.

2 DESCRIPTION OF THE SITE.

The investigation site is located at Huvudsta in Solna which is an urban district close to Stockholm (Figure 2.1). A blind road gives access to the site. The two boreholes ST1 and ST2 are situated at surface immediately above the intended extension of the tunnel. They are positioned at a distance of 2 m from each other and directed away from each other (Figure 2.2). The inclination of both boreholes is about 60^{o} below the horizontal plane (Appendix 1). The coordinates of the boreholes are given in a local coordinate system with the X-axis being the length coordinate along the tunnel. North of the local grid is directed N18E in relation to geographical north, i.e. perpendicular to the tunnel extension. The plane outlined by the boreholes is parallel to the planned tunnel extension. The tunnel will be located at a depth of 60 m at this site, which means that the distance between the intersections of the two holes with the tunnel will be approximately 70 m.

The site is located at the boundary of a large granitic outcrop close to a part of lake Mälaren. A fault striking NW and probably steeply dipping towards SW can be seen in form of a rock-face some tens of meters from the boreholes. ST2 is directed towards this fault.

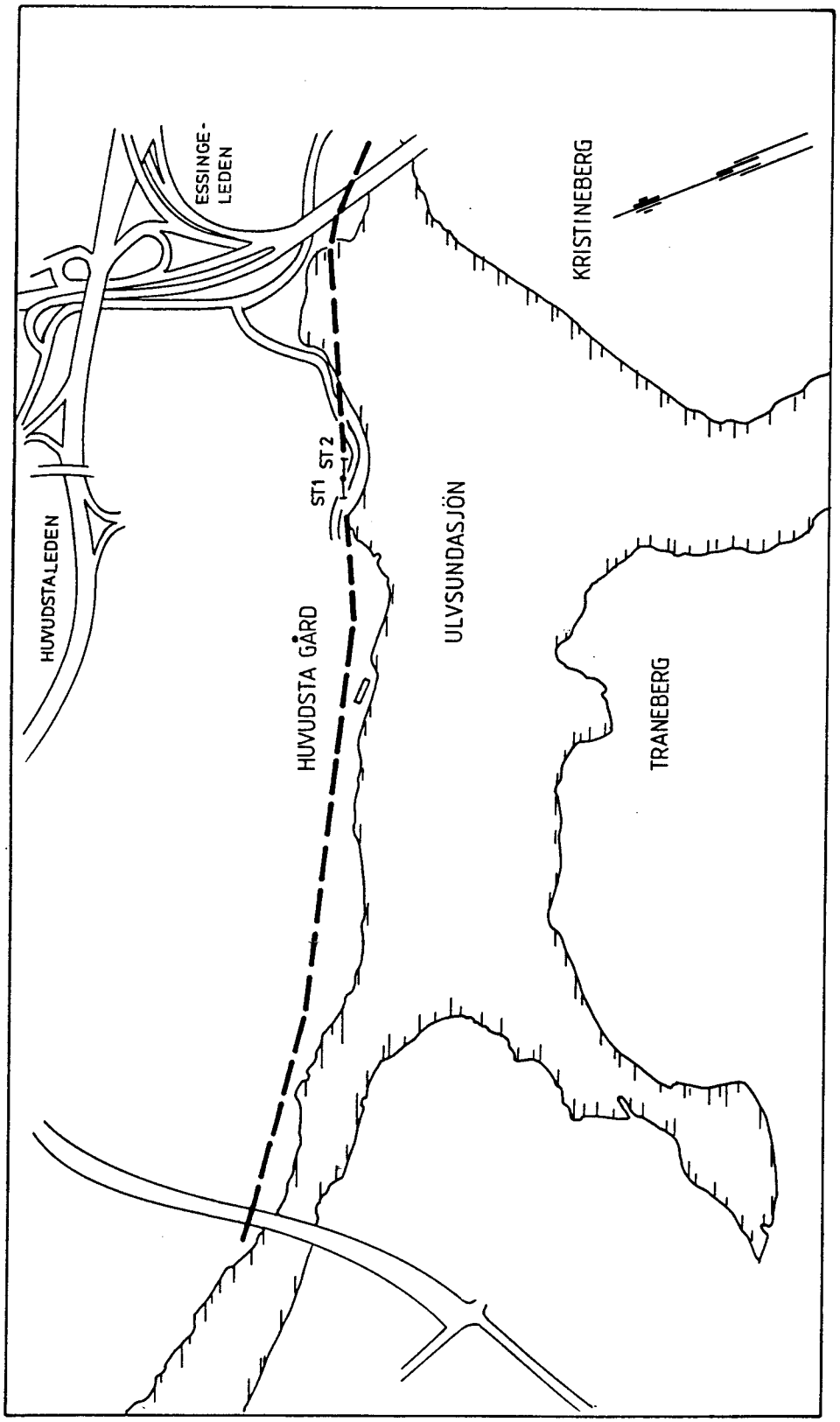

Figure 2.1 Location map of the Saltsjötunnel and position of boreholes ST1 and ST2. Tunnel is indicated by broken line.

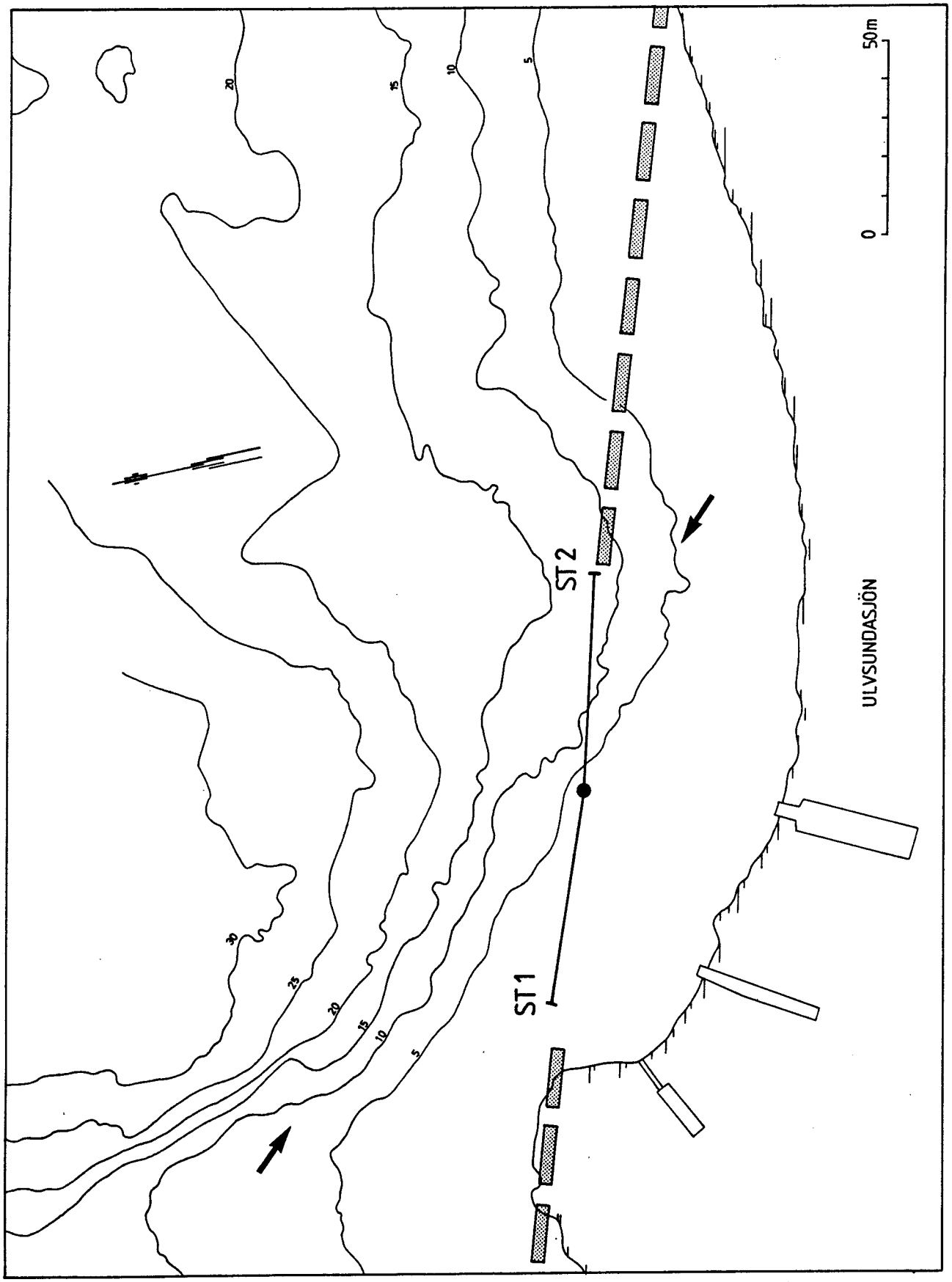

Figure 2.2 Detailed topographic map of investigated area and surroundings of boreholes ST1 and ST2 at the Saltsjötunnel. Arrows indicate steep rock-face.

3 INVESTIGATION PROGRAM

3.1 Geological core mapping

3.1.1 Drill core mapping

The core mapping of ST1 and ST2 were performed at SGAB´s core mapping facility in Uppsala.

The core boxes were put on a roller table to get an overview and to accomodate a measuring scale along the core. About 70 m of core could be on the table at the same time. The core mapping was performed by typing in the data on a microcomputer. The computerized core mapping system allows instant printout of a reference log.

The core is mapped fracture by fracture down the hole. Natural (coated) fractures are here defined as fractures with some kind of filling mineral or tempering that break the core into several pieces. Similar fractures that do not break the core are called sealed fractures. Fresh fractures are made by the drilling or handling of the core. Only the coated fractures are included in the statistics.

Fracture zones are sections that have more than 10 fractures per meter. Crushed zones are sections that are so intensely fractured that they can not be reconstructed. Statistically, crushed zones are assumed to have 50 fractures per meter.

The rock log refers to a user definable three letter code system. All observations are made with an accuracy of 5 cm.

The core in its boxes were photographed, in colour, both with dry and wet cores. The colour prints were then collected in a reference album.

Examples of core log and core log description are displayed in Figs. 3.1 and 3.1.

The following core mapping parameters were used:

Observation	Comment
Depth	5 cm accuracy
Rock type	three letter code
Fresh fracture	caused by drilling
Sealed fracture	does not break the core
Coated fracture	mineral coated
fracture angle to core axis	90 deg. is perpendicular to axis
fracture minerals	two letter code
fracture characteristics	slickensides etc.
Fracture zone	> 10 fractures/meter
fractures angles to core axis	90 deg. is perpendicular to axis
fractures minerals	two letter code
fractures characteristics	slickensides etc.
Crushed zone	unreconstructable core
fractures minerals	two letter code
fracture characteristics	slickensides etc.
Core loss	missing core
Uptake	fixed depth point
Comment	20 character note

Description

of the symbols and
codes on the core plot

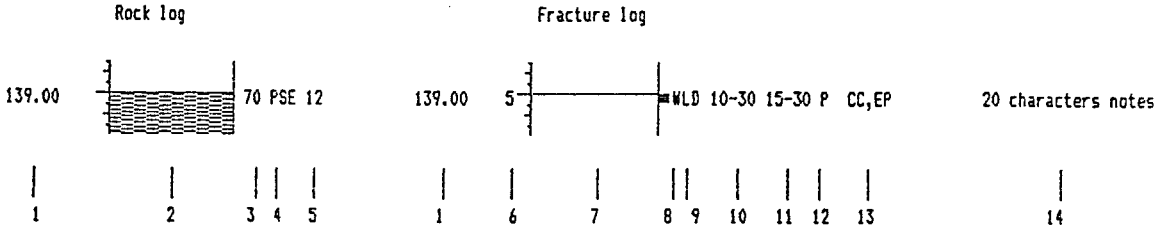

1 - Depth
2 - Marking for rock
3 - Angle
4 - Rock code
5 - Prefix code for rock
6 - Number of fractures
7 - Marking the type of observation
8 - Marking for uptake
9 - Marking for Weathered (W), Slickensides (L) and Dim (D)
10 - Angles from-to for parallel fractures
11 - Angles from-to for crossing fractures
12 - Marking for parallel foliation (P)
13 - Codes for 1-5 minerals
14 - Notes

Markings for fracture mapping

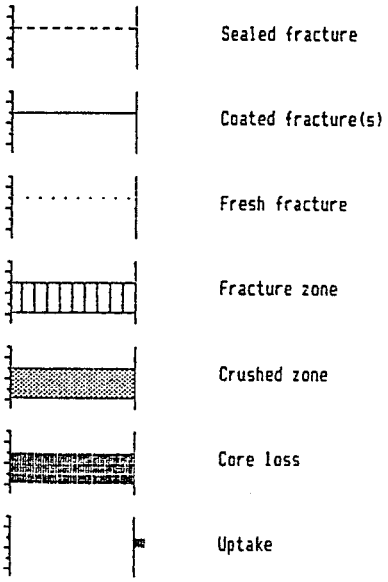

Fig 3.1 Example of core log from SKB core mapping system.

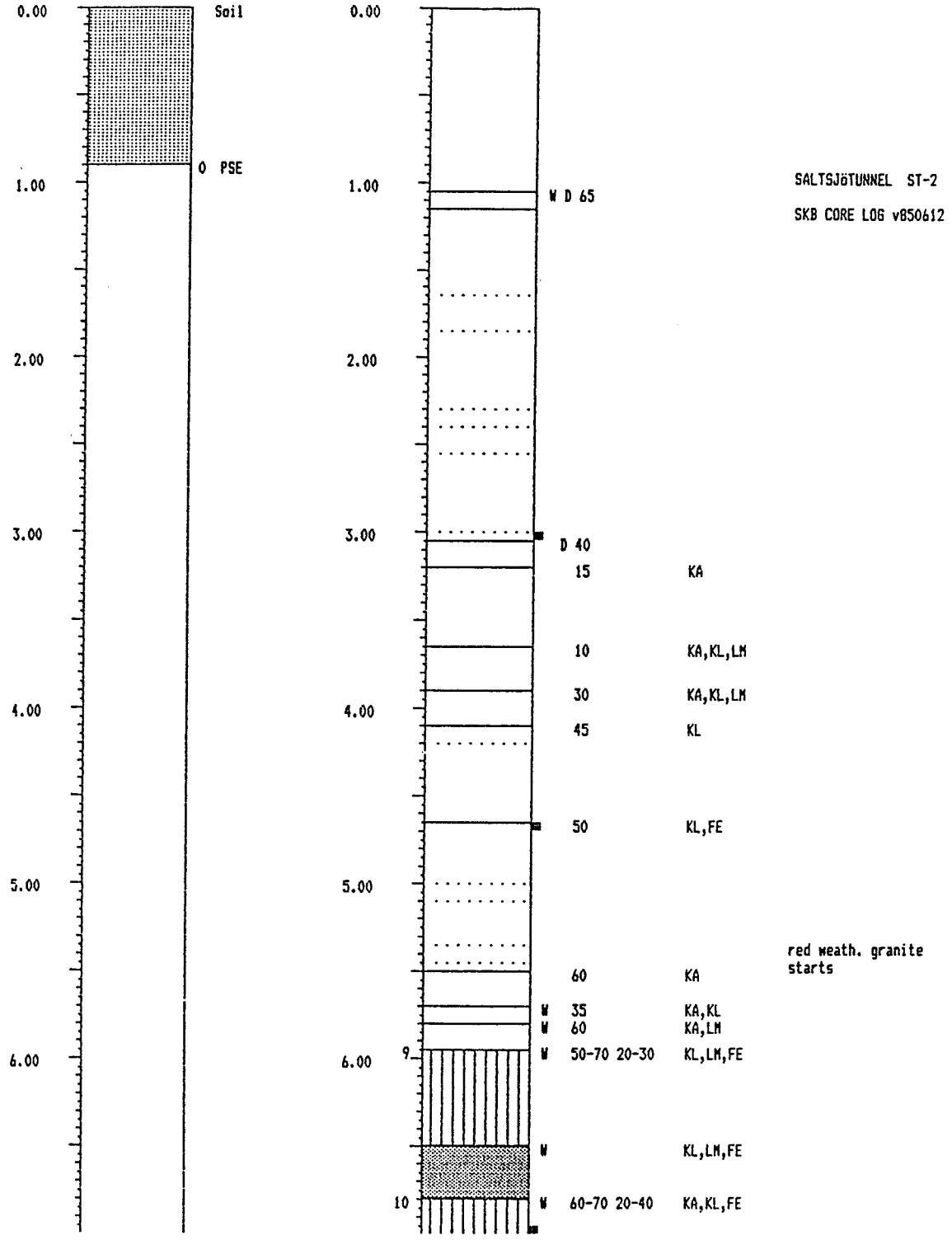

Fig 3.2 Example of core log description for SKB core mapping system.

3.1.2 Equipment for geological core mapping

The SKB (Swedish Nuclear Fuel and Waste Management Co) core mapping computer system was originally developed for registration of fracture observations made within the SKB site investigation and research and development projects. It has been used to map more than 25.000 m of core.

In this project the SKB core mapping computer system was used to record all core mapping data. The data is stored on 5 1/4 inch floppy discs. Transfering data to a main frame computer can be made simply.

The printed reference log is produced on an Epson MX-100 dot matrix printer. The system can produce ASCII-code files so that other computer programs can use data produced by the core mapping system.

3.2 Geophysical borehole logging

The geophysical borehole logging is performed in order to characterize the subsurface bedrock. Each separate log measures a physical property which is directly or indirectly related to the lithology and/or the fracturing of the bedrock, in the vicinity of the borehole. The collected logging data provides an interpretation including location of fractures/fracture zones and distribution of rock types. The recorded logs are presented in figures 4.3 and 4.4. These loggings results are used as reference material in the evaluation of the interpreted radar measurements.

3.2.1 Logging program and instruments

The geophysical logging operation, undertaken by Swedish Geological Co, were performed with the following methods:

* Natural gamma log
* Single point resistance
* Normal resistivity log
* Neutron log
* Temperature log
* Fluid resistivity log.

Also, the temperature gradient and the salinity of the borehole fluid were calculated from the temperature log and the temperature/ fluid resistivity logs, respectively.

This logging program is described below, but more detailed descriptions of the logging tools and their use can be found in Carlsten et al. (1985) and Almen et al. (1986).

Natural gamma log

The natural gamma activity of the bedrock will give information about the total radioactivity of the rock, i.e. the summation of potassium, uranium and thorium content. Variations in the concentrations of

these elements will normally correspond to mineralogical and lithological changes in the subsurface rock.

The probe, with an outer diameter of 42 mm, contains a scintillation detector. The active part is a 1" X 4" crystal of NaI(Tl), which is connected to a photomultiplier which transforms the light pulses created in the crystal to electrical signals proportional to the incoming gamma rays.

Single point resistance

The single point system has one downhole electrode and is used to measure the resistance of the formation around the electrode. The downhole electrode is combining both the current and the measurement electrode. The other electrodes are situated on the gound surface (one current electrode and one potential electrode), normally some 50 metres from the borehole.

The borehole probe consists of a plastic tube one meter in length with the electrode in the middle. The diameter of the probe is 53 mm and the length of the electrode is 50 mm.

The measuring volume of a point resistance system, contributing 90 % of the measurement is about 10 times the probe diameter. The measuring volume for the system is then about 50 cm. The single point resistance log has a high vertical resolution and is useful for detecting thin, narrow structures like fractures/fracture zones and dykes.

The single point resistance curve is presented in Ohms and the resistance ca be recorded at four different frequencies, namely; 3, 11, 33 and 110 Hz.

The point resistance log can also be corrected for variations in borehole diameter and fluid resistivity, using standard correction techniques.

Normal resistivity log

For the normal resistivity logs, a four electrode system is used to determine the resistivity of the bedrock. A and B are the current electrodes whilst M and N are the two electrodes between which the potential differences are measured.

Electrodes A and M are located on the probe while B and M are theoretically at a point infinitely distant from it, but in practice, normally some 50 metres from the borehole.

The distance, AM, is called the spacing (1.6 meter for this specific system) with the measuring point half-way between A and M.

The measuring volume for the normal resistivity configuration is approximately twice the electrode spacing (AM). The measuring volume for the 1.6 meter normal resistivity will roughly be a sphere with a radius of 325 cm.

Resistivity logs are recorded in Ohmmeters and the calibration on site is made by means of a variable resistor.

Resistivity logs can also be corrected for variations in borehole diameter and fluid resistivity, using standard correction techniques.

Neutron log

The recorded neutron log is roughly proportional to the porosity in sedimentary bedrock (i.e. the hydrogen content in the pore spaces). But the neutron tool also responds to bound water in shales which gives rise to an apparent high porosity for silt and shales. Also, the response from the neutron tool is affected by some elements with a high neutron cross-section, such as iron and chlorine.

In crystalline bedrock the porosities and thus the water content is very low (mostly less than 1 %). The neutron log is therefore sensitive to lithological/mineralogical variations in the bedrock.

The probe, outside diameter 54 mm, contains a radioactive 5 Ci

Am(Be)-241 source, which emits high energy neutrons into the formation. Two detectors (He-3) are positioned at a distance of 0.26 and 0.52 m from the source, respectively, and the instrument measures the amount of thermal neutrons present at the detectors.

The pulses from the two detectors are divided by a geometrical factor at the surface to compensate for geometrical spreading. The pulses from the closest spaced detectors are divided by 8 and the other by 4. The surface unit separates pulses from the two detectors and transforms the pulses into a DC-voltage proportional to the neutron counts.

The neutron-neutron probe is calibrated in calibration models with known porosity values and controlled water content in the pore spaces. When measuring in crystalline rock with low porosity values, the instrument is used to perform relative measurements since absolute calibration is impossible in this environment.

The results are often presented as the ratio of the counts at the front detector to the rear detector. It is also possible to present the results in counts/s or in porosity units, i.e. hydrogen index.

The measuring volume depends on the porosity and water content. The depth of investigation is approximately, (Serra, 1984):

60 cm with 0 % water
33 cm with 10 % water
25 cm with 20 % water
15 cm with 30 % water

Temperature log

The temperature of the borehole fluid will reflect the temperature of the surrounding bedrock, if the fluid has been static for a relatively long period. Water flow from fractures in or out of the borehole may be detected by variations/anomalies in the resultant temperature curve.

This instrument which has an outer diameter of 42 mm and is 106 cm

long, measures the temperature with a thermistor and presents the results in degrees Celsius. The calibration of the sensor, which has an absolute accuracy of 0.1 degree, is performed with a quartz thermometer. This calibration can be performed both in the laboratory and in the field.

The vertical temperature gradient is calculated from the temperature log in order to amplify the variations in the temperature log. The temperature gradient curve is presented in degrees Celsius/km.

Fluid resistivity log

The resistivity of the borehole fluid is determined with the fluid resistivity probe which consists of a five-electrode system situated in a plastic tube, open at both ends. The probe is 106 cm long and has an outside diameter of 42 mm.

The calibration of the fluid resistivity log is performed in a tank, filled with a water solution with very accurately determined salinity and temperature. During calibration, the salinity concentrations and/or the temperature are varied so that the system is calibrated for "normal" field conditions. The fluid resistivity results are presented in ohmmetres.

The results from the fluid resistivity log are, together with results from the temperature log, calculated to determine the salinity of the borehole fluid.

3.3 Hydraulic singlehole tests

3.3.1 Test program and interpretation

The tests were performed as singlehole injection tests with constant pressure using the Umbilical hose equipment (Almén et al., 1983). Firstly, the entire boreholes were logged with short-time tests (15 mins) using a packer spacing of 10 m (except the lowest interval). Subsequently, major parts of the boreholes were investigated with succesive tests using a packer spacing of 2 m. Selected borehole intervals were then investigated in detail with longer, transient tests (two hours of injection followed by two hours of recovery) using a packer spacing of 2 m:s. Also a spacing of 4 or 6 m was used. Finally a transient single-packer test of the entire borehole length was performed in each borehole. No crosshole hydraulic tests were carried out.

A preliminary hydraulic conductively value (KSS) was first calculated for each test using the simple expression:

$$KSS = \frac{Q_p}{L \cdot H_o} \qquad (1)$$

where Q_p = final flow rate (m^3/s)
L_p = packer spacing (m)
H_o = injection head (m)

From the injection phase the hydraulic conductivity (KI) may be calculated from the semi-log plot of 1/Q versus time (B3) from the following expression assuming (pseudo)-radial flow:

$$KI = \frac{0.183\ \rho\ g}{L \cdot \Delta(1/Q) \cdot dp} \qquad (2)$$

where ρ = density of water (kg/m^3)
g = acceleration of gravity (m/s^2)
$\Delta(1/Q)$ = change of reciprocal flow rate per cycle (s/m^3)
dp = injection pressure (Pa)

Despite the short test duration an (approximative) value of KI has also been determined from the short-time tests.

From the recovery phase of the transient tests the hydraulic conductivity (KU) may be calculated from the semi-log plot (C2) from the following expression assuming (pseudo)-radial flow:

$$KU = \frac{0.183\ Q_p\ \rho\ g}{L \cdot \Delta p} \qquad (3)$$

where Q_p = final flow rate (m^3/s)
Δp = change in pressure per log cycle (Pa)

For sections exhibiting a spherical flow response, approaching a steady-state flow rate during the injection phase, the preliminary value (KSS) is considered to be the best approximation of hydraulic conductivity. Also in sections where the flow rate and/or pressure is strongly fluctuating during the test and no well-defined straight line can be obtained the preliminary hydraulic conductivity value is used.

In order to make comparisons between tests in sections with different packer spacings the transmissivity T, defined as the product of the hydraulic conductivity and the packer spacing, has been calculated for each section. The lower measurement limit for the Umbilical system is considered at $T = 2 \times 10^{-10}\ m^2/s$. This value is based on a steady-state evaluation. From transient evaluation lower values

may occasionally be calculated since this method is based on the actual slope of a (semi-log) straight line. With a packer spacing of 2 m this value thus corresponds to a (steady-state) hydraulic conductivity of 10^{-10} m/s.

3.3.2 Equipment for hydraulic tests

The Umbilical hose system was used for all hydraulic tests performed. The field system uses two trailers, one for the instrumentation and the other for recording (Almen et al., 1983). All communication lines between the surface and the downhole tool are assembled in the Umbilical hose. The downhole tool can be separated in the following parts: packers, valves and pressure transducers (Figures 3.3 and 3.4).

The test section is straddeled by two packers separated by infiltration pipes. The packers are inflated by means of compressed air with water as the pressure transmitting medium. By closing the test valve the test section is confined. Water for injection is stored at the test site in 1 m^3-tanks and is filtrated before the tests. Before the test the entire injection system is pressurised down to the test valve. The injection test is started by opening the test valve and stopped by closing the valve.

The injection pressure, measured in the test section, is kept constant by regulating the air pressure in the water tank (computer-controlled system). The down-hole pressure is measured by two piezoresistive transducers. The temperature of the injection water at the surface is measured by a sensor. The flow rate is measured by two different flow meters, each representing different ranges, the first 0.09-7 l/min and the other 0-0.1 l/min.

The performance of a test is fully computer controlled. The test data is stored on floppy-discs. A plotter and printer is connected to the computer enabling the test data to be plotted in the field in various graphs.

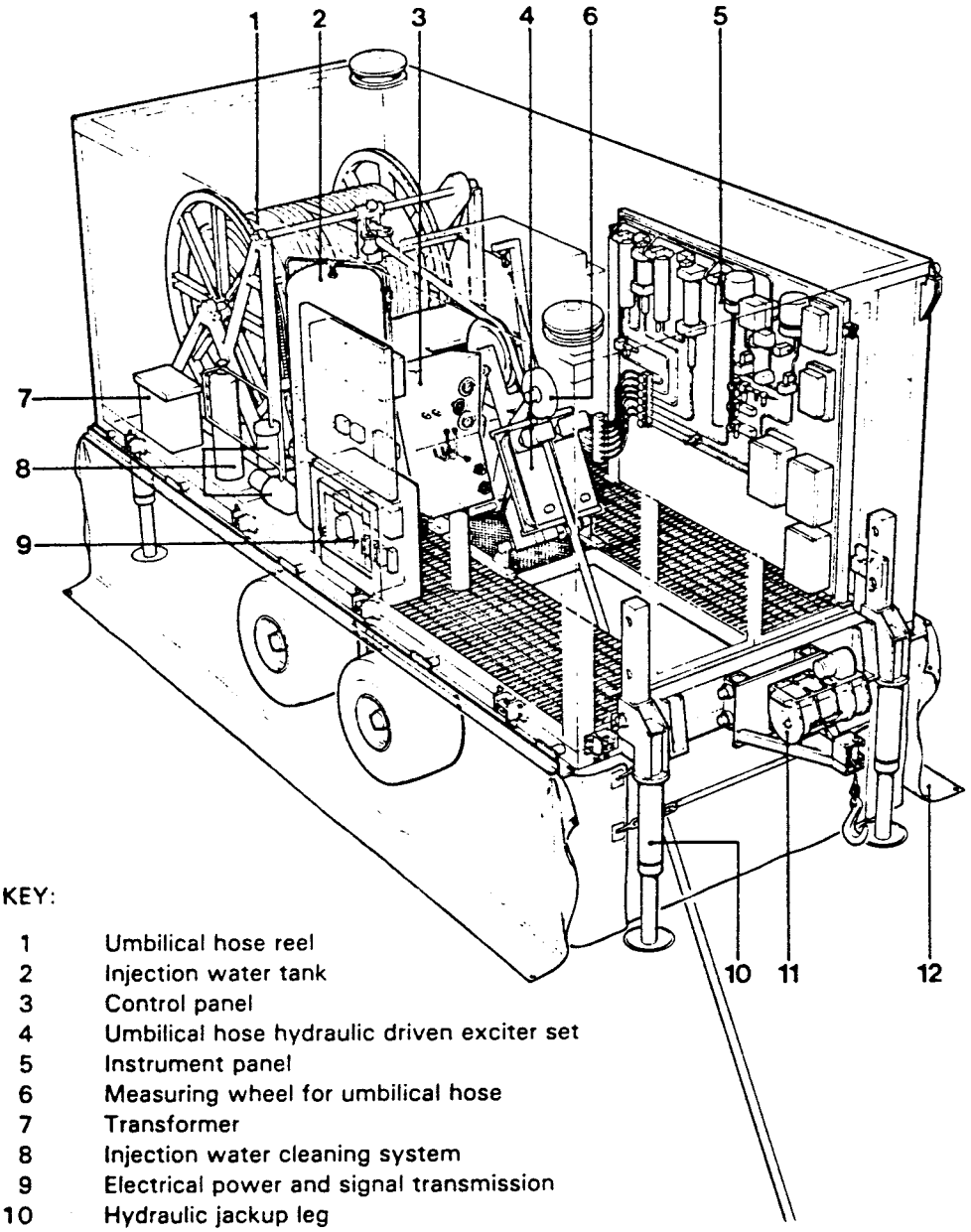

KEY:

1	Umbilical hose reel
2	Injection water tank
3	Control panel
4	Umbilical hose hydraulic driven exciter set
5	Instrument panel
6	Measuring wheel for umbilical hose
7	Transformer
8	Injection water cleaning system
9	Electrical power and signal transmission
10	Hydraulic jackup leg
11	Hydraulic winch
12	Thermal curtains

Figure 3.3 Principal overview of the measuring trailer.

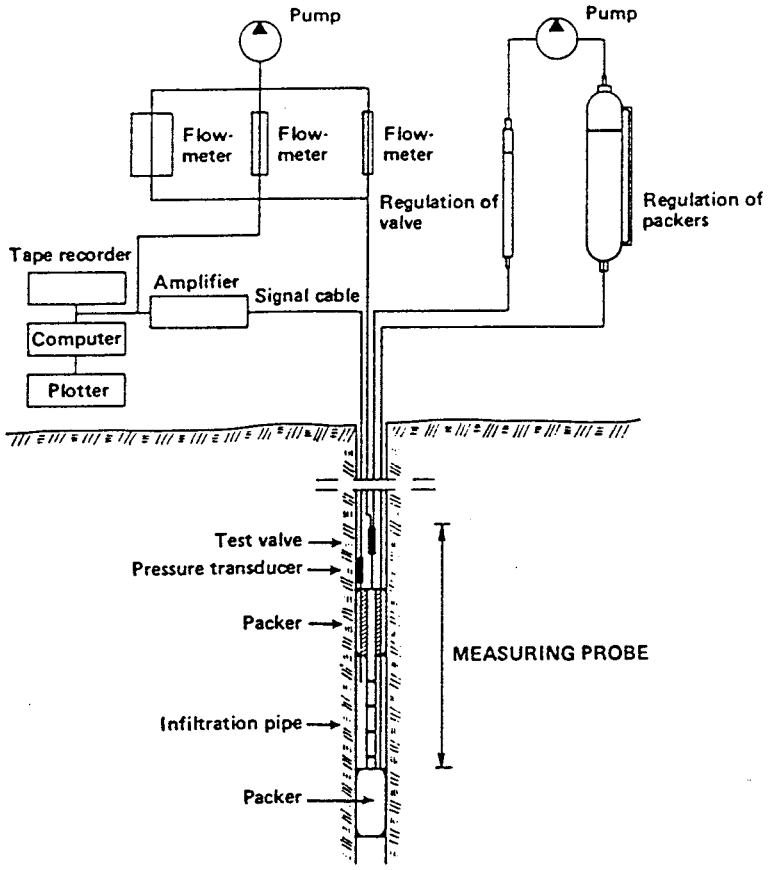

Figure 3.4 Principal overview of the umbilical hose system. configuration.

3.4 Borehole radar investigation

3.4.1 Radar measurement

The radar measurements in the boreholes at the investigation site comprise singlehole and crosshole measurements, performed with center frequency of 22 and 60 MHz.

Singlehole reflection measurements were made in each borehole with the center frequencies 22 MHz and 60 MHz. This means that four singlehole radar reflection measurements have been performed (Table 3.1). In a singlehole measurement the borehole radar probe consists of a transmitter and a receiver separated by glassfiber rods. The probe was in this case moved in 1 m steps. A sampling frequency of 245.1 MHz and 494.1 MHz was used for the 22 MHz and 60 MHz measurements, respectively. A total of 344 m of singlehole measurements were performed.

The crosshole measurements were also performed with the center frequencies 22 MHz and 60 MHz (Table 3.2). The crosshole measurements were carried out by first having the transmitter fixed at the starting position 20 m in ST1, while the receiver was moved in 4 m steps between 20-104 m in ST2. After the scan of the borehole ST2 had been completed the transmitter was moved 4 m downwards and fixed at 24 m in ST1, and the next borehole scan was performed by moving the receiver in 4 m steps from 104 m to 20 m. The procedure was repeated until the transmitter had been located at all positions with a 4 m interval in the borehole section between 20 m and 99 m (bottom) in ST1. A total of 21 borehole scans each consisting of 22 rays thereby resulted in a total number of 462 rays for the frequency 22 MHz. 16 borehole scans each consisting of 22 rays gave a total of 352 rays for the frequency 60 MHz. The smaller number of rays for the 60 MHz measurement was due to the high attenuation which resulted in that no signal could be registered for the largest source-receiver separations. Hence a measurement of the corresponding scans was not considered worth while.

The radar measurements were carried out during one week in December 1986.

Table 3.1 Measured intervals from singlehole radar reflection measurements.

	ST1	ST2	Transmitter-Receiver separation
22 MHz	2-87 m	10-89 m	15 m
60 MHz	3-92 m	2-93 m	9 m
Step	1 m	1 m	

Table 3.2 Measured borehole intervals for crosshole tomographic measurements.

	ST1 Transmitter	ST2 Receiver
22 MHz	20-99 m*	20-104 m
60 MHz	20-80 m	20-104 m
Step	4 m	4 m

* Step between 96-99 m is only 3 m.

3.4.2 Equipment for borehole radar investigation

A short pulse borehole radar system has been used for the radar measurements. The system was originally developed by the Swedish Geological Co. (SGAB) as a part of the International Stripa Project. A continued development to make the system adapted for field work on a production basis has later been funded by SKB.

The radar system consists of four different parts;

- a microcomputer with two 5 inch floppy disc units for control of measurements, data storage, data presentation and signal analysis.

- a control unit for timing control, storage and stacking of single radar measurements.

- a borehole transmitter for generation of short radar pulses.

- a borehole receiver for detection and digitization of radar pulses.

The radar system works in principle in the following manner: A short current pulse is fed to the transmitter antenna, which generates a radar pulse that propagates through the rock. The pulse is made as short as possible to obtain high resolution. The pulse is received by the same type of antenna, amplified, and registered as a function of time. The receiver may be located in the same borehole as the transmitter or in any other borehole. From the full wave record of the signal the distance (travel time) to a reflector, the strength of the reflection, and the attenuation and delay of the direct wave between transmitter and receiver may be deduced.

The recording of the signal is similar to that of a sampling oscilloscope, i.e. for each pulse from the transmitter only one sample of the received electric signal is taken at a specific

time. When the next pulse is generated a new sample is taken which is displaced slightly in time. Thus, after a number of samples a replica of the entire signal is recorded. The sampling frequency and the length and position of the sampled time interval can be set by the operator.

Optical fibers are used for transmission of trig signals from the computer to the borehole probes and for transmission of data from the receiver to the control unit. The optical fibers have no electrical conductivity and will not support waves propagating along the borehole. Another advantage of optical fibers is that they can not pick up electrical noise and as the signal is digitized down-hole there will be no deterioration of the signal along the cable. The quality of the results will thus be independent of cable length.

There is no direct connection between the transmitter and the receiver. Both probes are instead connected directly to the control unit and the transmitter and the receiver can be put into the same as well as into separate holes. In other words, the radar may be used for both singlehole and crosshole measurements. The system also provides absolute timing of the transmitted pulses and a calibrated gain in the receiver which makes it possible to measure the travel time and the amplitude of the radar pulses in a crosshole measurement and hence provide data for a tomographic analysis.

A block diagram of the control unit, transmitter and receiver is shown in Fig. 3.5 and the technical specifications of the system are given in Table 3.3.

Table 3.3 Technical specifications of the borehole radar system

General	
Frequency range	20-80 MHz
Total dynamic range	150 dB
Sampling time accuracy	1 ns
Maximum optical fiber length	1000 m
Maximum operating pressure	100 Bar
Outer diameter of transmitter/receiver	48 mm
Minimum borehole diameter	56 mm
Transmitter	
Peak power	500 W
Operating time	10 h
Length	4.8 m
Weight	16 kg
Receiver	
Bandwidth	10-200 MHz
A/D converter	16 bit
Least significant bit at antenna terminals	1 uV
Data transmission rate	1.2 MB
Operating time	10 h
Length	5.4 m
Weight	18 kg
Control unit	
Microprocessor	RCA 1806
Clock frequency	5 MHz
Pulse repetition frequency	43.1 kHz
Sampling frequency	30-1000 MHz
No of samples	256-4096
No of stacks	1-32767
Time window	0-11 us

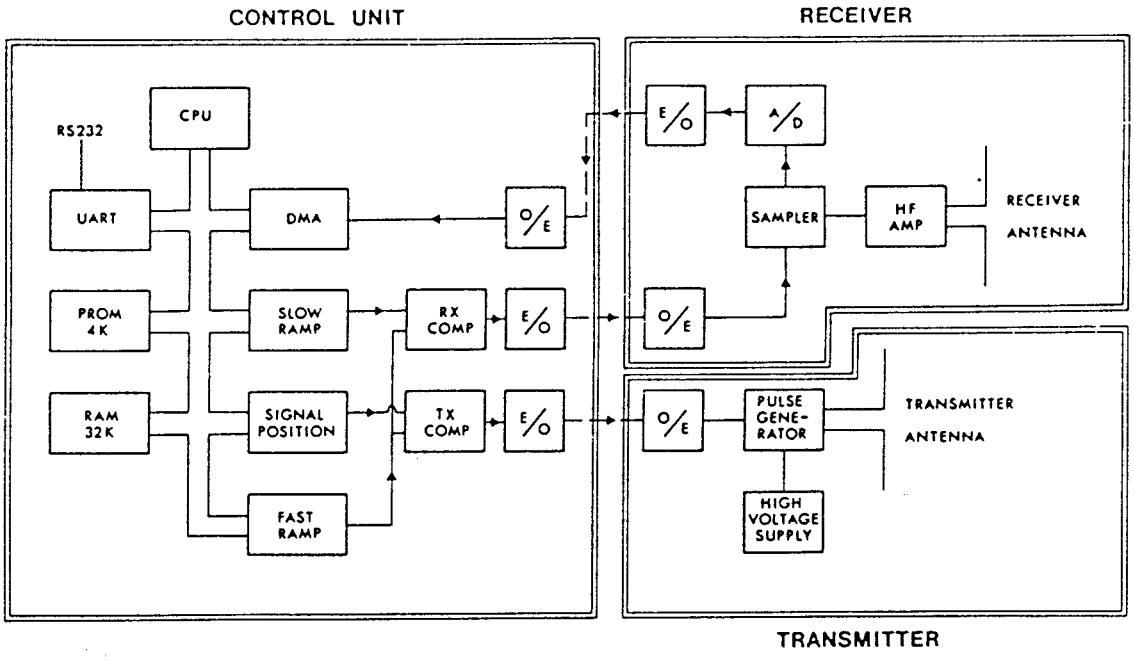

Figure 3.5 Block diagram of the borehole radar system.

4 GENERAL RESULTS OF THE BOREHOLE INVESTIGATIONS

In the following chapters 4.1 - 4.4 are the results from the different investigations presented individually. Definitions of used terms for the different investigation methods are presented in Table 4.1.

Table 4.1 Nomenclature and definition for the different investigation methods.

Investigation method	Abbreviation of interpreted features	Nomenclature	Definition
Geological core mapping	G1-G6	Fracture zones	>10 fractures/m in the core.
Geophysical logging	P1-P11	Fractures/ fracture zones	Low resistivity and high neutron ratio.
Singlehole radar	1-x	Structures.	Reflexes and/or loss of radar pulse energy.
Crosshole radar	A-E	Structures.	High attenuation of radar waves. Slowness of radar wave velocity.
Combined interpret.	I-III	Zones	Detected by most of the investigation methods and considered prominent.

4.1 Geological core mapping

The core logs for ST1 and ST2 are published in Stråhle (1987).

The site consists essentially of two rock types, grey fine to medium grained granite and grey medium to coarse grained migmatite. The granite, i.e. the Stockholm granite, is homogeneous and shows only weak foliation. The migmatite, i.e. migmatite gneiss, is veined and rather coarse. The origin is presumably a greywacke. According to the regional geological map the strike of the migmatite in the investigation area and its surroundings is NNW and the dip 80-85 degrees towards E (Stålhös,1969).

A condensed rock log, fracture densities and different fracture mineral densities from the core mapping of the boreholes are displayed in Figs. 4.1 and 4.2. Detected zones are presented in Table 4.2.

ST1, the borehole directed towards west, shows two distinct fracture zones. The zones are named G1 and G2.

G1 (4.90-7.65 m) shows foliated, cataclastic, red coloured and altered rock. This zone has a maximum fracture density of 14 fractures per meter. Chlorite, calcite and oxidized iron minerals occurs on the fracture faces which also show signs of alteration.

G2 (32.85-37.50 m) shows tectonized, brecciated, red coloured and altered rock. The maximum fracture density of this zone is 27 fractures per meter. Chlorite, calcite and oxidized iron minerals occurs on the fracture faces which also show signs of alteration.

ST2, the borehole directed towards east, shows four more or less distinct fracture zones. They are named G3, G4, G5 and G6.

G3 (5.35-8.25 m) shows red oxidized granite with calcite, chlorite and oxidized iron minerals on the fracture faces. The zone has a maximum fracture density of 49 fractures per meter. The centre of the zone is belived to be at about 6.65 meters.

Table 4.2 Geologically detected zones and their characteristics in boreholes ST1 and ST2.

Zone	Depth	Red col.	Minerals	Crush.	Max.frac frequency	Other
ST1						
G1	4.90-7.65	yes	KL,KA,FE	no	14	cataclase
G2	32.85-37.50	yes	KL,KA,FE	yes	27	breccia
ST2						
G3	5.35-8.25	yes	KL,KA,FE	yes	49	tectonite
G4	41.70-49.50	yes	KL,KA,FE	yes	23	mylonite
G5	68.35-70.80	yes	KL,KA	no	14	
G6	79.90-82.60	yes	KL,KA	yes	18	tectonite

G4 (41.70-49.50 m) is probably two zones according to the two peaks in the fracture density. Two oxidized zones are also detected at 43.10 m and 48.30 m. A 5 mm wide calcite sealed mylonite occurs at 38 m. The two zones consist partly of red oxidized and crushed migmatite with chlorite, calcite and iron oxides on the fracture faces. The maximum fracture densities are 23 and 15 fractures per meter. The center of the two zones is supposed to be around 44 m.

G5 (68.35-70.80 m) shows a minor fracture zone with alteration and 20 cm of red coloured rock. The zone also shows an accumulation of chlorite. Maximum fracture density is 14 fractures per meter.

G6 (79.90-82.60 m) consists of, as G5, a minor fracture zone with red coloured rock and alteration. The maximum fracture density is 18 fractures per meter.

Fracture densities have been calculated for the different rock types in ST1 and ST2. The result is shown in Table 4.3. The table shows

Table 4.3 Fracture densities for the different rock types in the boreholes ST1 and ST2.

Rock type	Length (m)	Number of fractures	Fract./m
ST1			
Migmatite	54.75	290	5.30
Pegmatite	1.30	3	2.31
Granite	53.15	205	3.86
ST1 total	109.20	498	4.86
ST2			
Migmatite	62.70	419	6.68
Pegmatite	5.10	35	6.86
Granite	41.30	186	4.50
ST2 total	109.10	640	5.87

that migmatite and granite occupy roughly the same length in ST1 while migmatite is more common in ST2. Pegmatite constitute a larger part of the core in ST2 compared to ST1. The mean fracture frequency in ST2 is higher than in ST1. Migmatite seems to be more fractured than granite in general in both boreholes. Pegmatite in ST1 exhibits the lowest fracture frequency encountered and the highest in ST2.

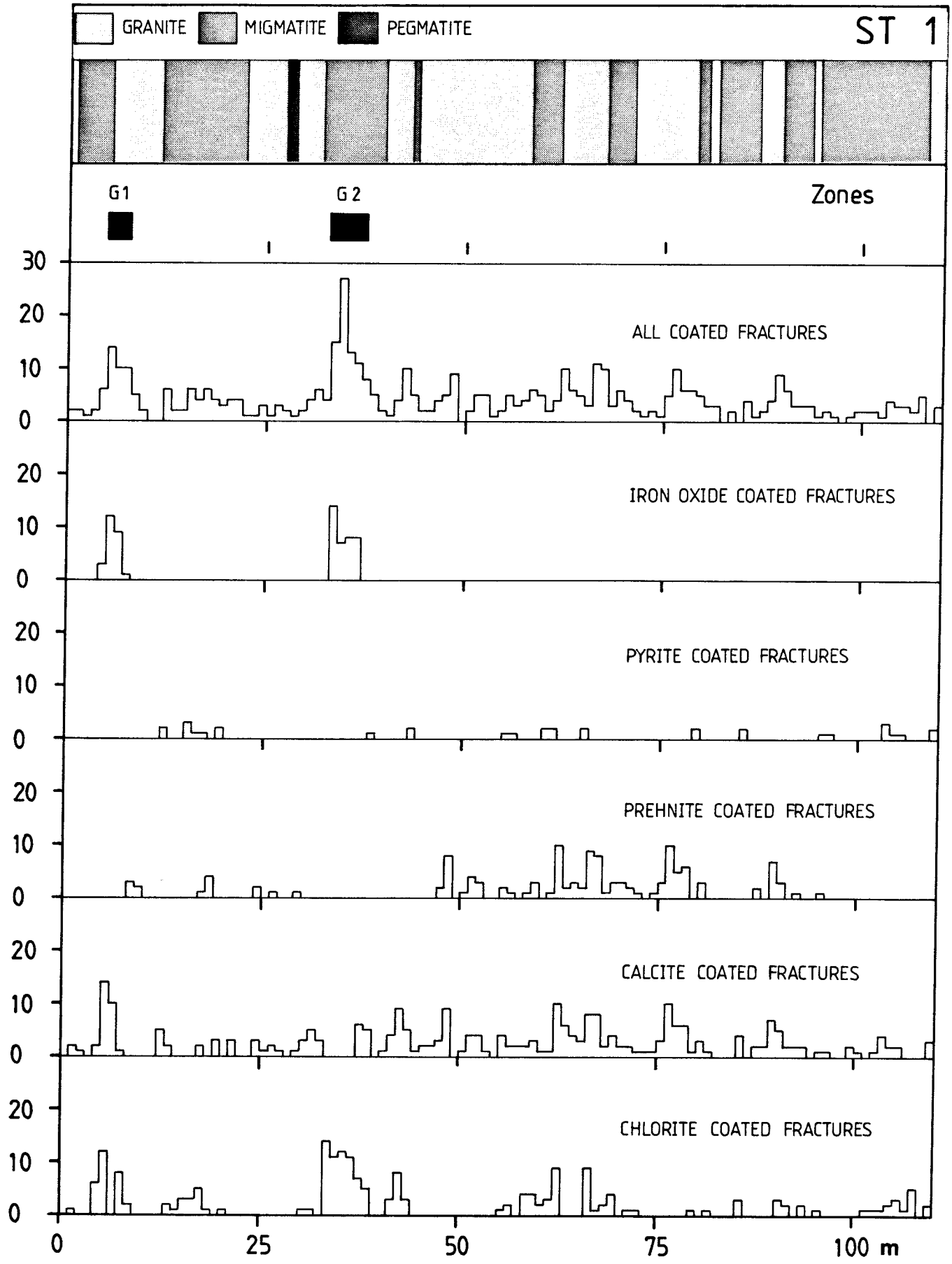

Figure 4.1 Condensed rock log, fracture densities and different fracture mineral densities from the core mapping of borehole ST1.

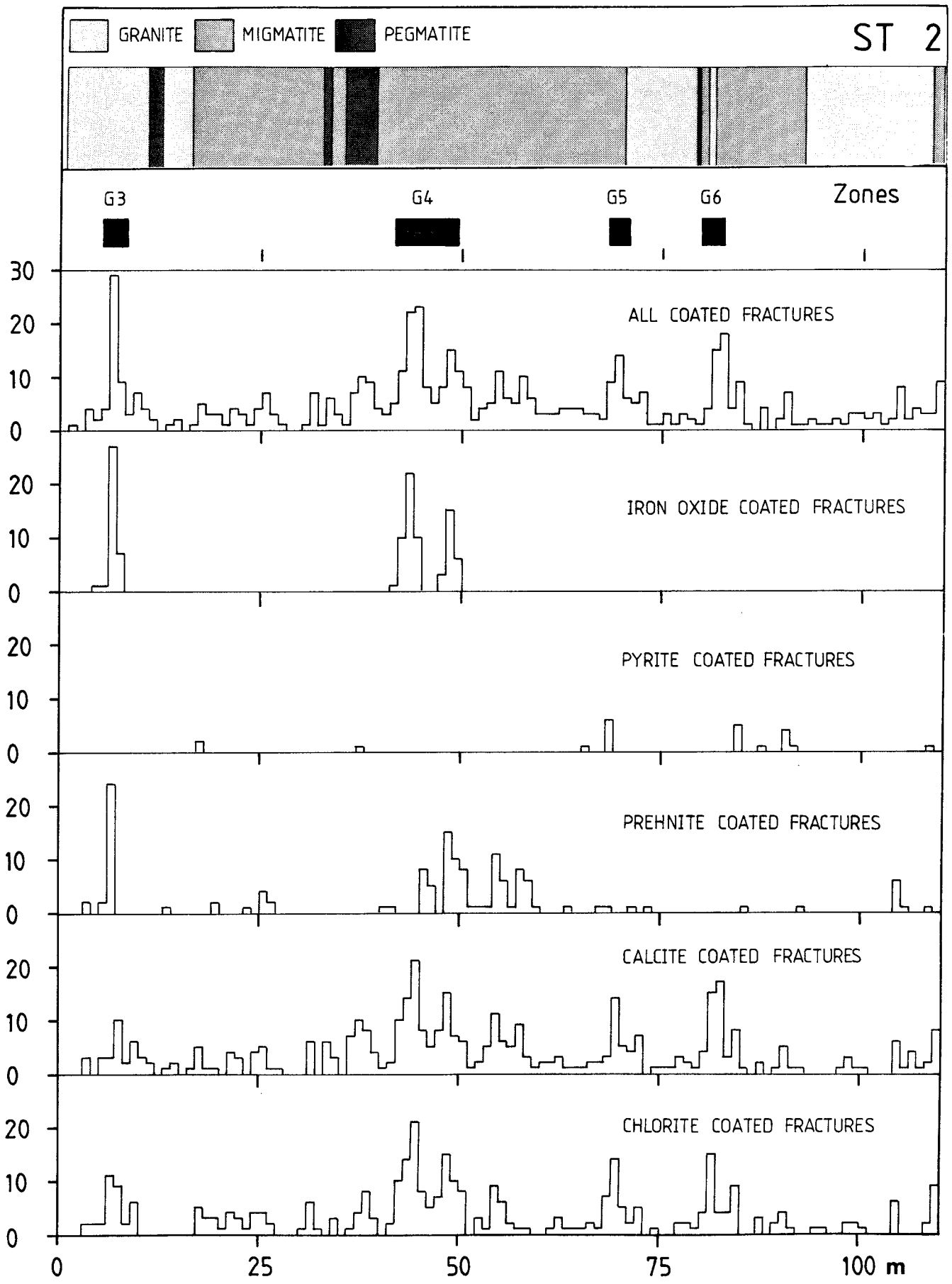

Figure 4.2 Condensed rock log, fracture densities and different fracture minerals densities from the core mapping of borehole ST2.

4.2 Geophysical borehole logging

In the two boreholes ST1 and ST2 the following geophysical logs were performed:

* Natural gamma log
* Single point resistance log
* Normal resistivity log
* Neutron log
* Temperature log
* Borehole fluid resistivity log

Also, the temperature gradient and the salinity of the borehole fluid were calculated from the temperature log and the temperature/fluid resistivity logs, respectively. The recorded logs are presented in Figs. 4.3 and 4.4.

A combined interpretation of the geophysical logs performed within this project gives information on both the bedrock lithology and the fractures/fracture zones intersected by the boreholes. The lithology within this bedrock complex consists of granite, migmatite and pegmatite. No effort has been made to present the geophysical interpretation verbally, meter for meter, down the boreholes in text. Instead, the general characterization and criteria for the respective bedrock masses and fractures/fracture zones, are described below. The detailed geophysical interpretation, following the described criteria, are presented visually in Figs. 5.1 and 5.2, where location and type of rock and/or fracture zones are shown. Also, the interpreted fracture zones are presented in Table 4.4, where they have been given the abbreviation P.

The geophysical logs reveal that the rock mass within the investigated area is complex with sections of granite, migmatite and pegmatite intersecting each other. The bedrock is in many cases fractured in the vicinity of the rock contacts forming the fracture pattern showed in Figs 5.1 and 5.2. From the logs it can be deduced that the rock mass towards the bottom of the boreholes has fewer and smaller fractures/fracture zones. There is also indications showing that the rock mass around borehole ST2 is more fractured than ST1.

The granite in the investigated area is, as seen from the log results (Fig 4.3 and 4.4), characterized by an average natural gamma activity of about 40-50 microRoentgen/h and by a recorded resistivity indicating an average level of about 50 000 ohmm, measured with the normal resistivity configuration. Both the gamma activity and the resistivity shows "normal" levels and ranges compared to granites encountered elsewhere in Sweden. From the resistivity measurements performed in borehole ST1 one can observe a distinct drop in the average resistivity levels between the uppermost section, above 32 m, and the underlying sections, below 39 m. These phenomena can be correlated to the salinity of the borehole fluid, which increases between 32 to 39 m thus causing the drop in the resistivity measurements. The marked increase in salinity around the section 32-39 m in ST1 indicates water flow in this fracture zone. The neutron log results are sensitive to water content/porosity variations but also sensitive to lithological/mineralogical variations and the results hence supports the lithological interpretation. The recorded neutron ratio in the granite is generally higher that the neutron ratio encountered in the pegmatite and lower than the neutron ratio measured in the migmatite.

The migmatite is characterized by an average level of the natural gamma activity of about 30 microRoentgen/h, which is lower than the activity in the granite. This is interpreted to be caused by the generally lesser content of potassium in migmatite compared to granite. The resistivity in the migmatite sections are roughly of the same order as for the granite. The recorded neutron ratio is higher than the neutron ratio measured in the granite. The higher neutron ratio in the migmatite is interpreted to be caused by the higher amount of dark, mafic minerals generally observed within the migmatites. The mafic minerals contain (amongst others) elements like iron, chlorine and manganese which has a "high thermal neutron absorption cross section" giving rise to an apparent high porosity (neutron ratio).

The pegmatite is determined from the high natural gamma activity, compared to the granite and the migmatite. The gamma activity is more than 50 microRoentgen/h with a recorded top value of about 75 microRoentgen/h. This high activity is caused by the high potassium

content, normally encountered within pegmatites. The resistivity of the pegmatite sections are of the same order as the other bedrock sections within this investigated area. The recorded neutron ratio in the pegmatite is lower than in both the granite and the migmatite. This is interpreted to be due to the absence of dark, mafic minerals, within the pegmatite.

The fractures/fracture zones are, from the combined geophysical logging results, characterized and determined by the relatively low resistivity and the relatively high neutron ratio (apparent porosity). The decrease of the resistivity in the fractures/fracture zones are caused by the increased water content or coatings/infillings on/in the fractures, such as chlorite and clay. Due to the higher resolution of the single point resistance, compared with the normal resistivity log, the single point resistance log is more useful for detecting fractures/fracture zones. The increased water content, together with chlorite, clay etc., also gives rise to a higher neutron ratio (apparent porosity), which generally can be observed on the neutron logs from the two respective boreholes.

Table 4.4. Fracture zones as interpreted from the geophysical logging.The presented resistivity and neutron ratio are relative classifications of the recorded response, for each zone.

Hole	Zone	Location (m)	Resistivity	Neutron ratio	Comments
ST1	P1	6.5- 8.0	very low	high	same as zone P5
ST1	P2	32.0-39.0	very low	very high	same as P7/P8
ST1	P3	61.5-66.5	very low	high	
ST1	P4	75.5-78.0	very low	high	same as zone P11
ST2	P5	5.5- 7.5	very low	high	same as zone P1
ST2	P6	20.5-25.5	low	high	
ST2	P7	41.0-46.5	very low	very high	same as zone P2
ST2	P8	47.5-49.5	very low	high	same as zone P2
ST2	P9	53.5-55.0	low	high	
ST2	P10	69.0-70.5	low	high	
ST2	P11	81.5-83.0	very low	very high	same as zone P4

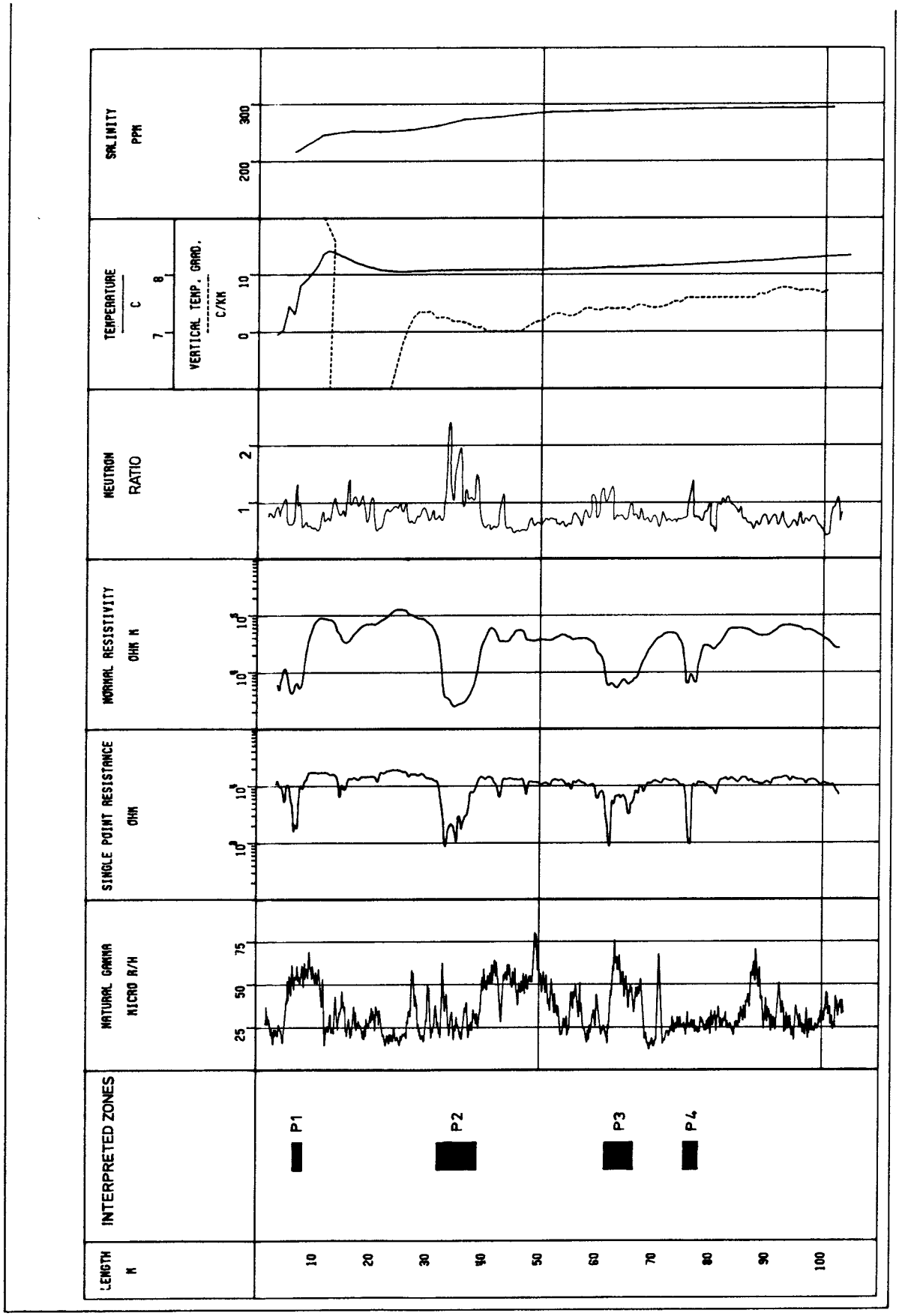

Figure 4.3 Results from the geophysical borehole measurements in ST1.

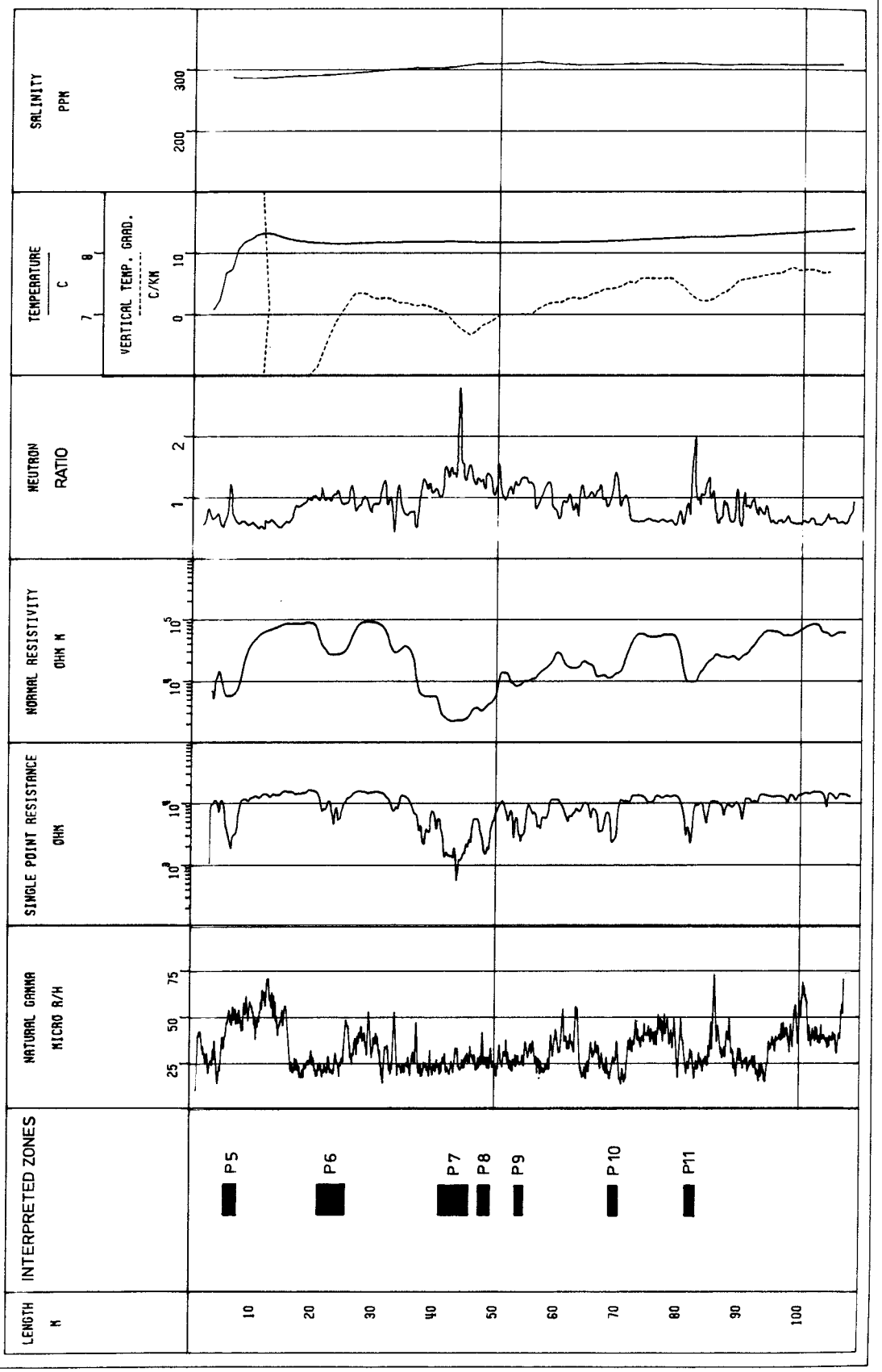

Figure 4.4 Results from the geophysical borehole measurements in ST2.

4.3 Hydraulic singlehole tests

The results of the hydraulic 10 m-tests are presented graphically in Figs. 4.5 and 4.6. These figures show the transmissivity versus depth in the two boreholes. The transmissivity calculated from the 2 m-tests and the single-packer tests is also presented in these figures.

As can be seen from Fig. 4.5 the highest transmissivity values in borehole ST1 are found in sections 5-15 m, 29-31 m, 33-35 m and 77-81 m. Also the interval 45-65 m shows high transmissivity. In borehole ST2 high transmissivities are obtained in sections 5-15 m, 41-43 m, 43-45 m, 71-73 m, 77-79 m and 81-83 m.

The general trend of transmissivity versus depth is somewhat different for the two boreholes. The decrease of transmissivity versus depth is more pronounced in borehole ST1. The deeper part of borehole ST2 (below 65 m) in general has a significantly higher transmissivity than in ST1, particularly in the sections 71-73, 77-79 and 81-83 m.

The relatively sharp contrast in calculated transmissivities between successive 2 m sections is pronounced in both boreholes. The calculated transmissivities for longer test sections show in general good agreement with the sum of transmissivities for shorter subsections. No information on the interconnectivity between the boreholes can be obtained from the hydraulic tests performed. To investigate the hydraulic connection directly, crosshole hydraulic tests would be required.

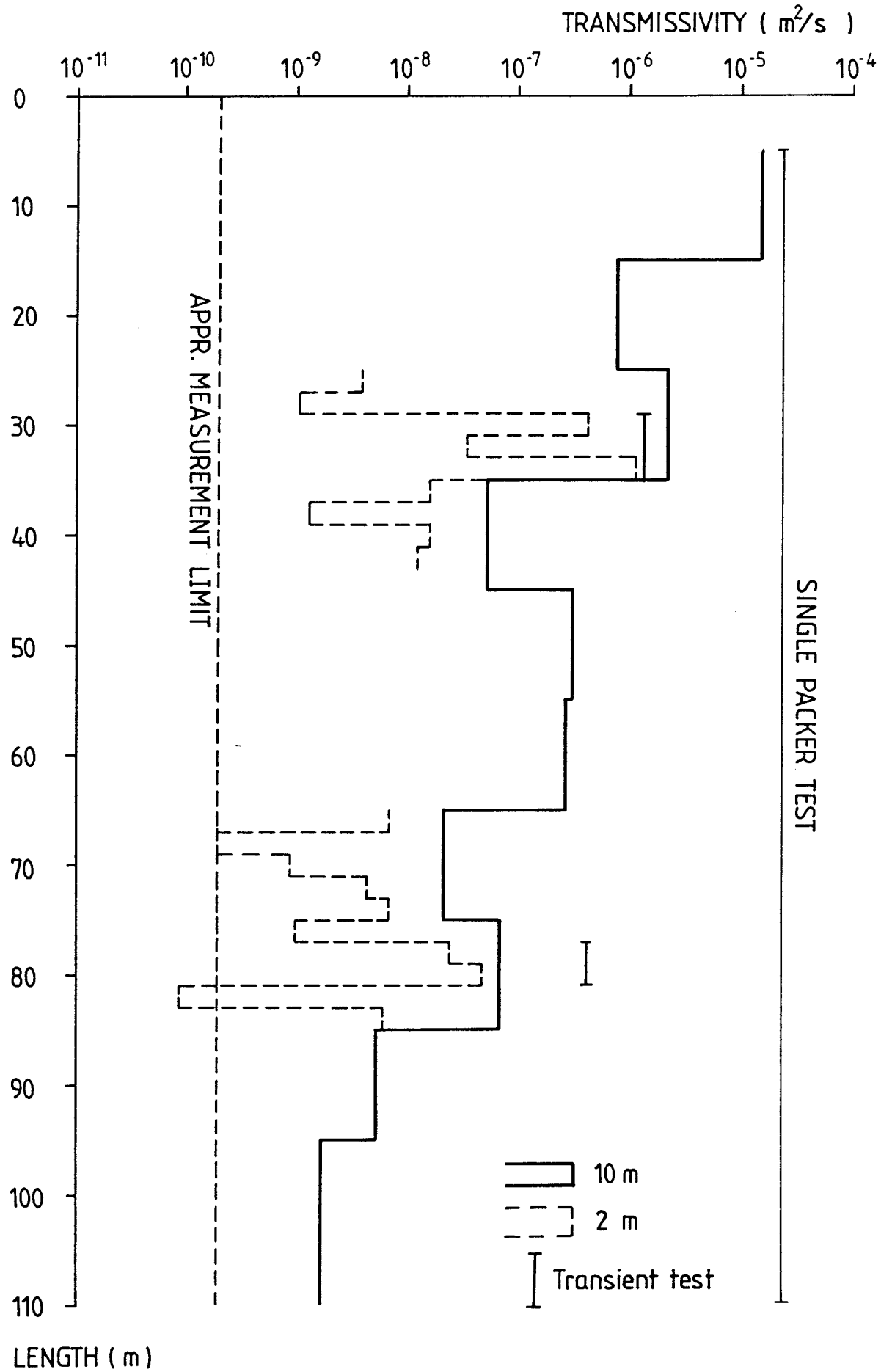

Figure 4.5 Transmissivity measured in 10 m and 2 m sections versus depth in borehole ST1.

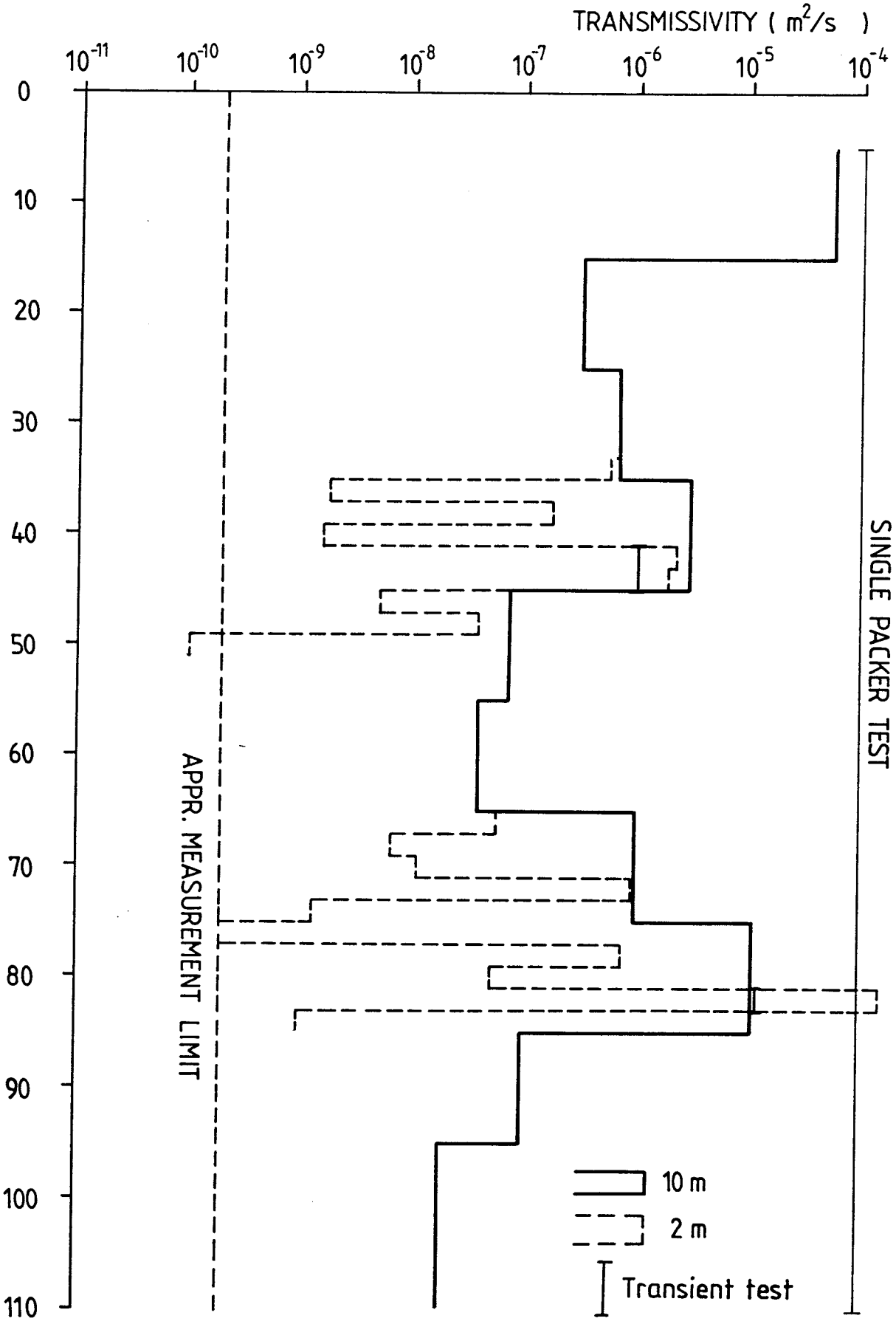

Figure 4.6 Transmissivity measured in 10 m and 2 m sections versus depth in borehole ST2.

4.4 Borehole radar investigation

The radar model of the site is obtained mainly from a combination of the data from the single hole reflection measurements and the results of the amplitude tomography. The results from the crosshole reflections have not contributed much to the interpretation of the radar model, due to the high attenuation at the site, and is therefore not included separately in this report.

The 60 MHz radar map from ST1 exhibits 16 reflections with small angle (20-35^{o}) to the borehole axis (Figure 4.7 and Table 4.5). A majority of the reflections are more or less parallel to each other thus indicating a pattern of parallel structures in the rock mass. All reflections are considered to be part of or associated with a marked, steep rock-face striking NW (geographic north) shown in Fig.2.2. One reflection in the radar map has a significantly different orientation, namely 50^{o} to borehole axis. This reflection is interpreted to represent a part of the subhorizontal structure A.

The 22 MHz radar map from ST1 exhibits a similar pattern of structures with a small angle to the borehole axis (Figure 4.8 and Table 4.6). However, one reflection exhibits an angle of 50^{o} to borehole axis, this corresponds to a similar reflection in the 60 MHz radar map.

The 60 MHz radar map from ST2 exhibits 17 reflections which all are interpreted as vertical or subvertical structures (Figure 4.9 and Table 4.7). All of them are interpreted as parallel structures associated with the steep rock-face striking NW mentioned above.

The 22 MHz radar map from borehole ST2 exhibits a similar pattern of structures with acute angles to the borehole axis (Figure 4.10 and Table 4.8). Exceptions are two reflections which have a somewhat larger angle of 40^{o} to borehole axis. Both structures are interpreted as representing parts of the subhorizontal structure A.

The sections which exhibit loss of radar pulse energy occur in all four radar maps, and they are interpreted to represent the subhorizontal structure A (Table 4.9). In ST1 there is also a similar

but weaker section in the 22 MHz map which might represent a part of the vertical structure B. The reflections associated with these sections are rather weak and are sometimes not seen at all.

A majority of the singlehole reflections intersect the boreholes with an angle in the interval 25-35^{o}. Most of these reflections are more or less parallel to each other and consequently they are considered to belong to the same structural feature. There is a small difference in the average angles determined in the two different measured frequencies. The average angle of radar reflecting planes to the borehole in ST1 and ST2 from the 22 MHz measurement is between 30^{o}-35^{o} while the angle from the 60 MHz measurement is close to 25^{o}.

A plot in a Wulff net of the singlehole data gives three possible orientations for the major structure set; one set striking roughly N-S (in the local grid system) with an almost vertical dip, two sets striking E-W (local grid) with dips of about 50^{o} towards North and South, respectively. Taking the following description of the tomograms and singlehole radar into account, the first vertical set is considered best suitable.

The result of the singlehole radar measurement is combined with the tomographic analysis and presented below. The tomograms are presented in Figs 4.11 and 4.12 which also shows the resulting radar model. It should be noted that the presented radar model is a conciliation of the interpretation of the tomograms and singlehole radar, and smaller discrepancies might occur.

Structure A appears as a horizontal feature in the tomogram. It is interpreted as being the structure connecting the part of the borehole where the radar pulse energy losses are significant in the singlehole reflection measurements, but the structure does not exhibit distinct reflections. The crosshole data shows that the structure is penetrated by both boreholes at the depth interpreted from the single hole measurements. It has not been possible to determine the dip of structure A with any accuracy but the most probable interpretation is that the structure is semihorizontal.

Structure B appears with a steep dip in the tomogram. The

intersection with borehole ST1 between 50-63 m is determined from the singlehole reflection measurement. The most probable strike of the structure is NW which roughly corresponds to a marked feature in the topography.

In the tomogram structure C seems to have a steep dip above a vertical depth of 50 m and below that depth the dip is reduced. The crosshole reflection data indicate a slightly different location and orientation for the structure. From that data it appears to intersect ST2 at a depth of 25-35 m and to have a dip of about 60^{o}. From the singlehole reflection measurement this section is represented by one reflection, namely no.2 (22 MHz) indicating a dip of 35^{o} to borehole axis. The strike of the structure should be approximately perpendicular to the plane of the boreholes. A dip of 60^{o} is roughly in correspondance with the dip indicated in the tomogram at a depth below 50 m. The crosshole reflection data also indicates that at least two structures with different orientations intersect ST2 at about 40 m.

Based on the results from the singlehole reflection data structure D is thought to be steeply dipping. It can be assumed that it is more or less parallel with structure B and C.

Structure E appears with a steep dip in the travel time tomogram. It can be treated as parallel to structure B. Its existence is supported by the 60 MHz single hole measurement as two reflections intersecting at 74 m in ST1, with an angle of 25^{o} and 18^{o}, respectively. This would imply a vertical dip of the structure.

A general feature of the obtained tomograms is the relatively larger attenuation and slowness in the Western part of the investigated borehole section between structures B and C. The rock is in these parts (i.e. between tunnel coordinates 1700 m to about 1750 m) expected to be more fractured and altered than in the remaining parts of the investigated length of the tunnel.

In Table 4.10 is the location, orientation and intersection with the tunnel of the five most prominent structures encountered in the radar investigation presented. Fig. 4.13 shows the calculated intersection with the tunnel of radar interpreted structures. One should keep in

mind that the coordinates are not exact, especially not for structure C which is inclined and thereby a small change in the dip gives a considerable change in the intersection with the tunnel.

The attenuation of the radar waves at this site is considerably higher than what has been obtained at most other radar investigated sites. This generally indicates a high level of fracturing and alteration. In this area, the high attenuation is probably related to the complex rock mass containing several contacts between different rock types.

Table 4.5 Radar reflecting structures identified from borehole ST1 (60 MHz).

Position (m)	Reflector (no.)	Angle Upp/Low	Comments
-26	10	/25	Above boreh.
			Three parallel struct.
-18	9	/25	Above boreh.
-10	8	/23	Above boreh.
7	1	/30	
28	15	/25	
35	2	50/	Horizontal structure.
51	17	20/	Same as 18.
51	18	/20	Same as 17.
62	13	/15	
70	3	25/	Same as 16.
71	16	/18	Same as 3.
79	14	25/	
94	4	20/	
96	11	25/	Undulating
103	5	25/	
124	6	23/	Below boreh.
137	7	21/	Below boreh.
			Four parallel struct.

Table 4.6 Radar reflecting structures identified from borehole ST1 (22 MHz).

Position (m)	Reflector (no.)	Angle Upp/Low	Comments
-20	10	/38	Above boreh.Two parall.
-17	9	/30	Above boreh.
-5	8	/30	Above boreh.
7	1	/30	
36	12	/25	
38	2	50/	Horizontal structure.
62	13	/30	Same as 3.
71	3	35/	Same as 13.
72	14	50/	
94	4	20/	
101	11	33/	
106	5	40/	
113	6	40/	Below boreh.
142	7	30/	Below boreh. Four parallel struct.

Table 4.7 Radar reflecting structures identified from borehole ST2 (60 MHz).

Position (m)	Reflector (no.)	Angle Upp/Low	Comments
2	1	/20	
1	13	/25	
41	3	23/	Same as 10.
41	10	/24	Same as 3.
56	16	18/	Same as 12.
56	12	/18	Same as 16.
64	18	/15	Same as 17.
67	17	20/	Same as 18.
71	19	21/	
87	20	20/	
89	4	30/	
101	14	25/	
109	11	25/	
127	5	30/	Below boreh.
150	8	20/	Below boreh.
159	6	20/	Below boreh.
162	7	25/	Below boreh.

Table 4.8 Radar reflecting structures identified from borehole ST2 (22 MHz).

Position (m)	Reflector (no.)	Angle Upp/Low	Comments
-3	1	/25	
-1	13	/45	Above boreh.
25	2	/35	
39	9	40/	Horiz.struct.Same as 10.
39	10	/35	Horiz.struct. Same as 9.
47	3	40/	Horizontal struct.
58	12	/35	
90	4	40/	
112	11	30/	
116	5	40/	Below boreh.
132	8	35/	Below boreh.
146	6	35/	Below boreh.
176	7	25/	Below boreh.

Table 4.9 Sections with loss of radar pulse energy in the boreholes ST1 and ST2 (22 and 60 MHz).

	ST1	ST2
Loss of pulse energy (22 MHz)	29-41 m 65-69 m	34-49 m
Loss of pulse energy (60 MHz)	28-39 m	36-46 m

Table 4.10 Orientation, location and intersection with the tunnel of the most prominent structures encountered in the radar investigations. Strike and coordinates are given in the local grid.

Structure	Orientation	ST1	ST2	Tunnel
A	Semi-horizontal	28-41	34-49	Parallel
B	NW/vertical	50-63	-	1702-1705
C	N/60E	-	25-35	1739-1760
D	N-NW/vertical	-	107-109	1796-1802
E	N-NW/vertical	73-75	-	1698-1700

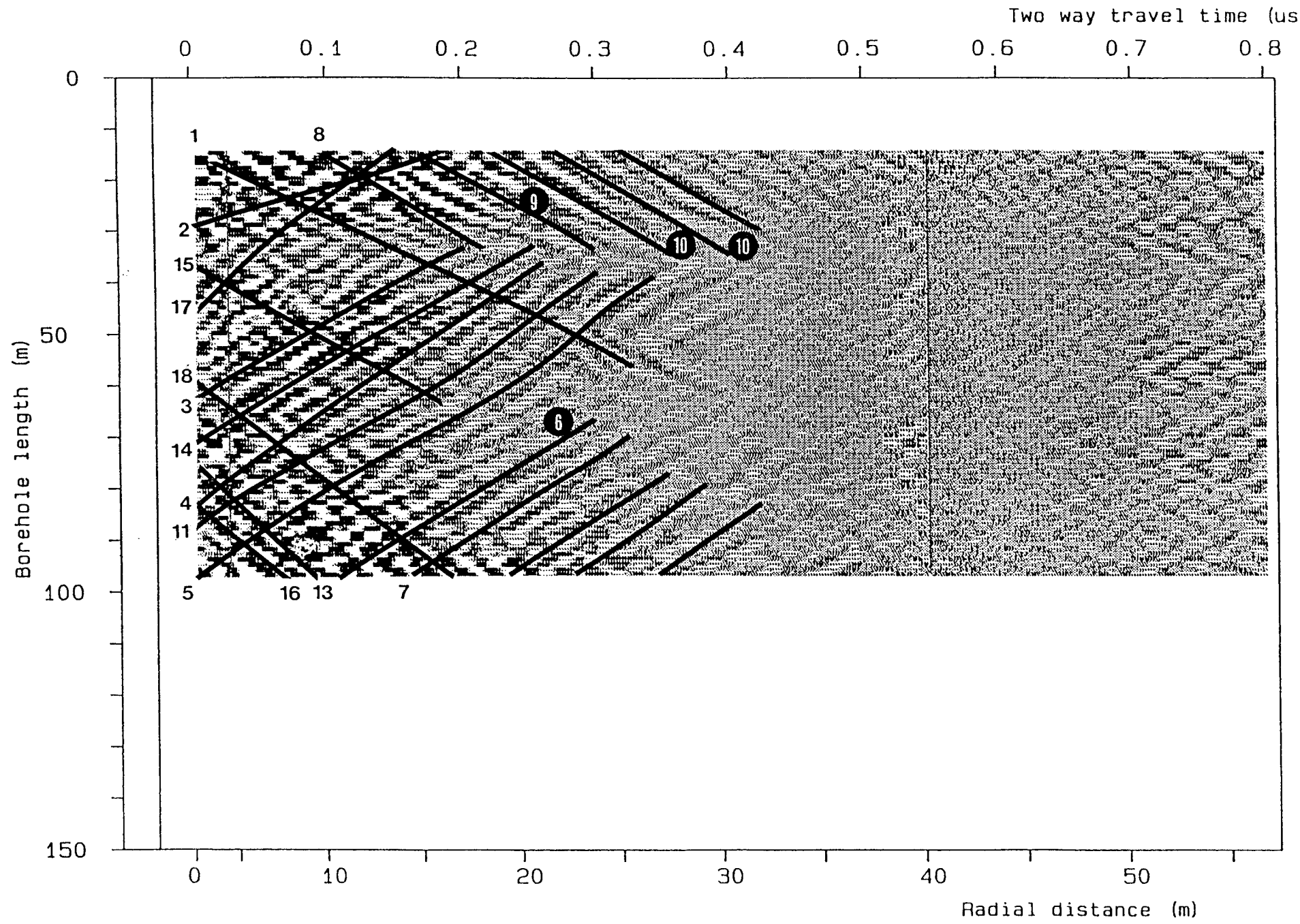

Figure 4.7 Radar map for borehole ST1, 60 MHz.

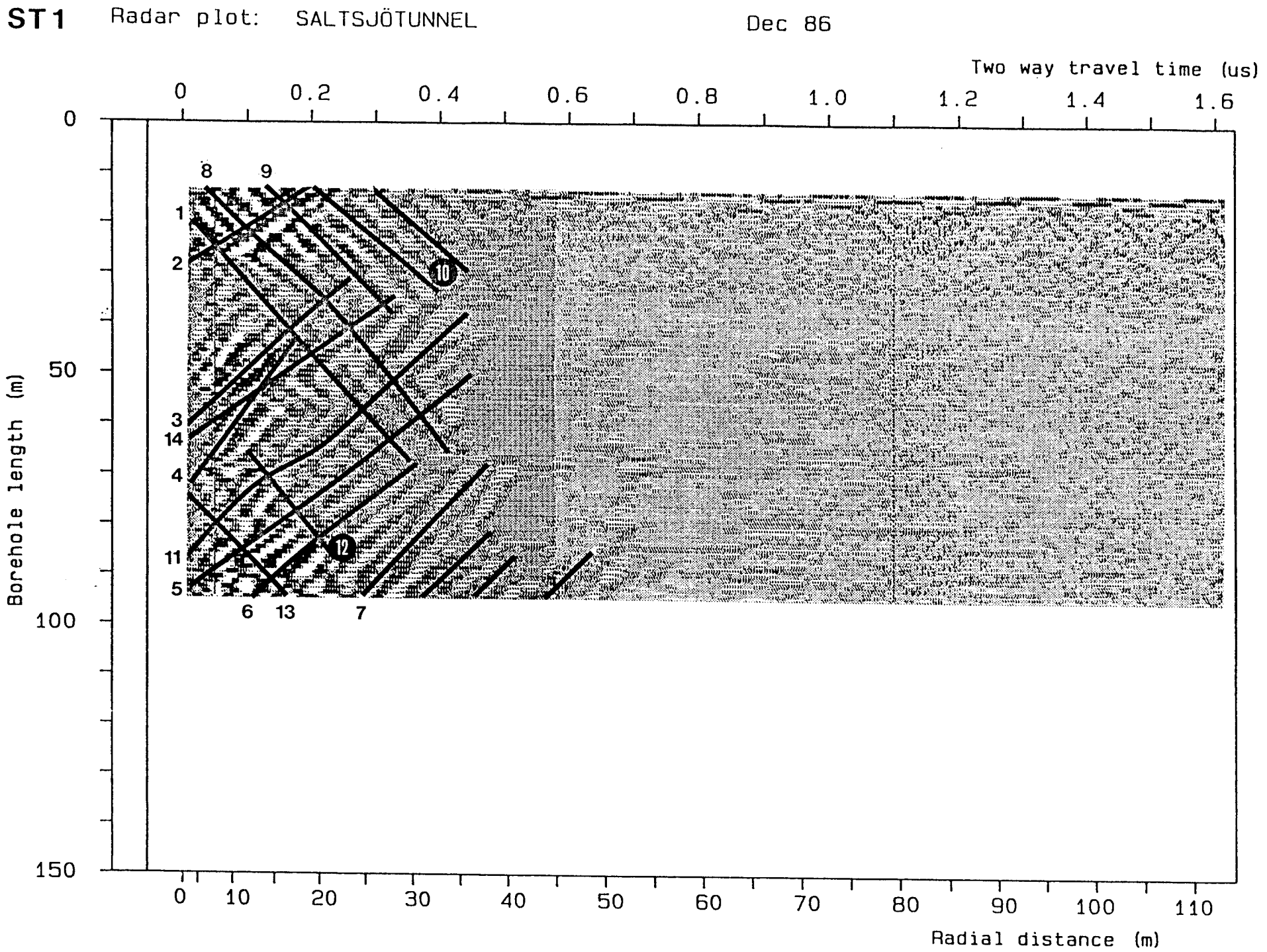

Figure 4.8 Radar map for borehole ST1, 22 MHz.

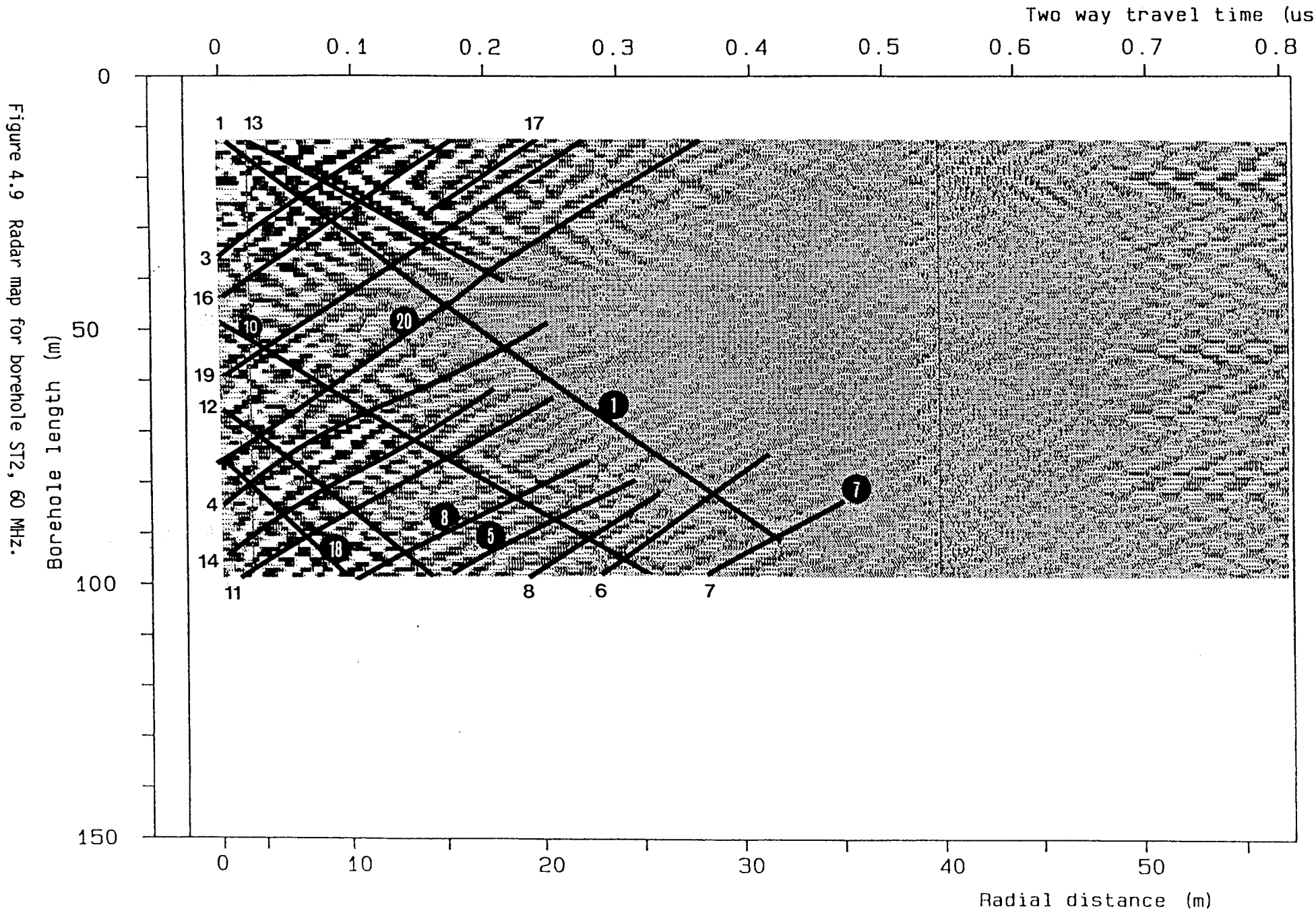

Figure 4.9 Radar map for borehole ST2, 60 MHz.

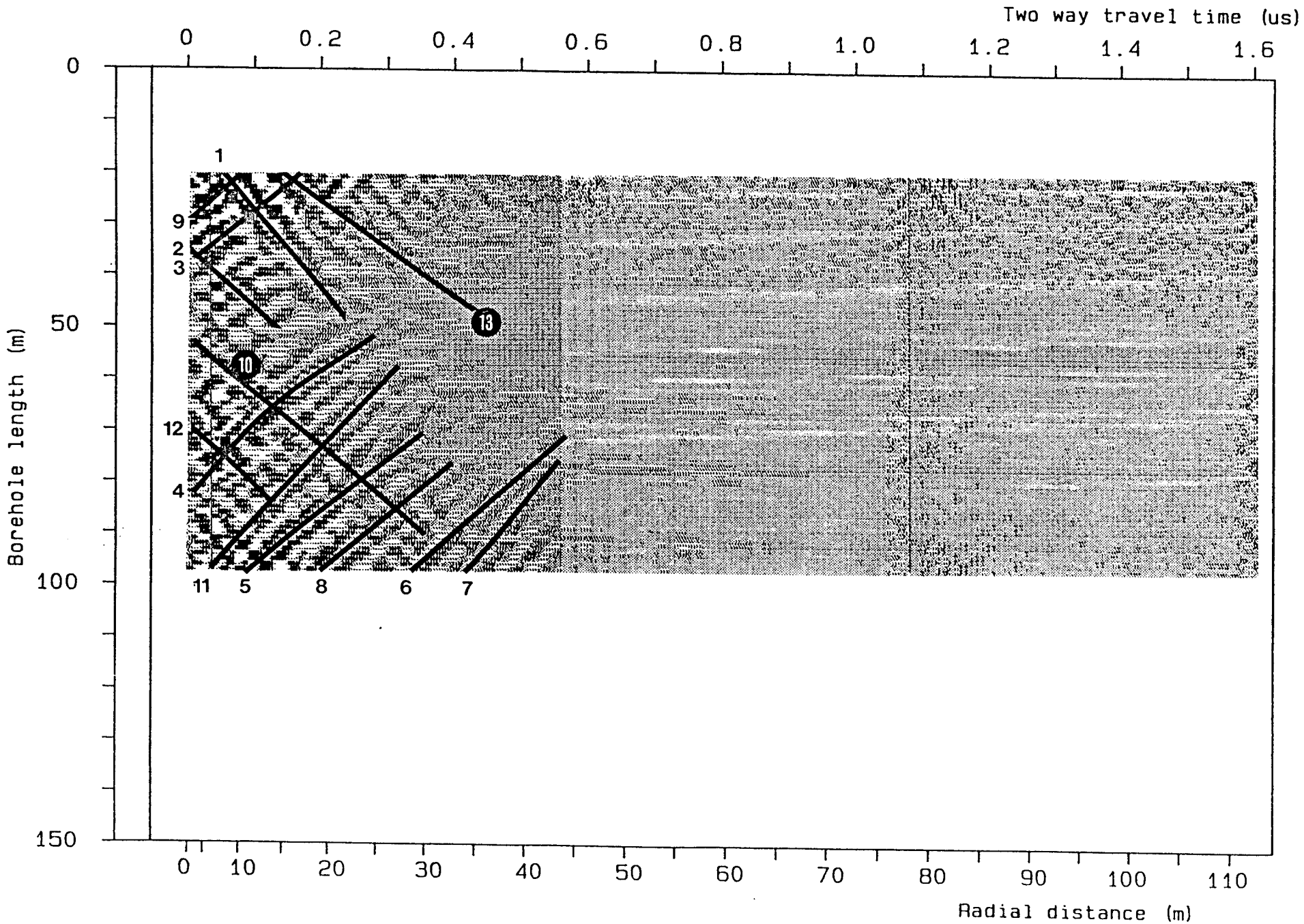

Figure 4.10 Radar map for borehole ST2, 22 MHz.

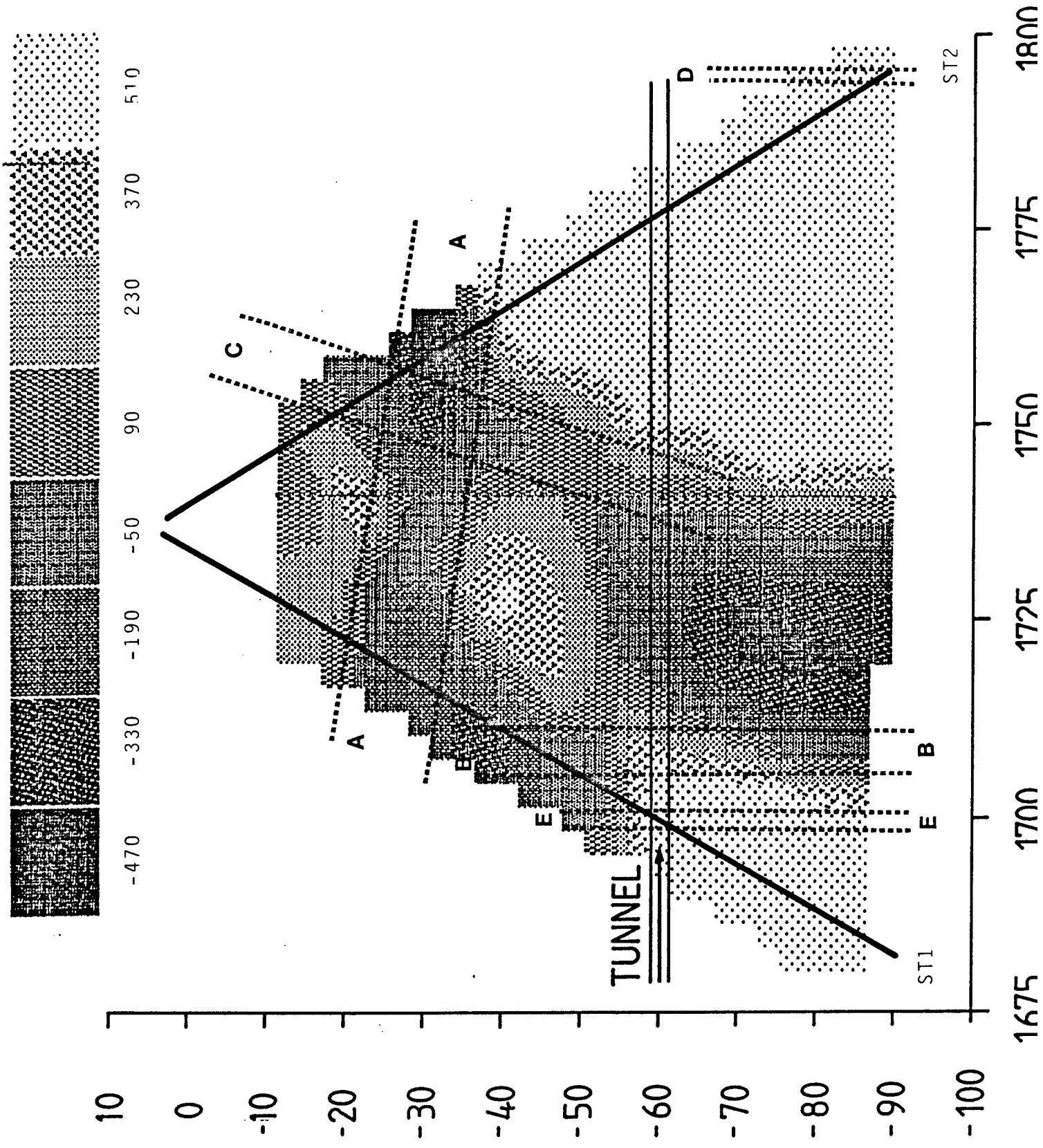

Figure 4.11 Radar tomogram showing the distribution of radar attenuation in the plane between the boreholes obtained at the crosshole measurements between ST1 and ST2 at a center frequency of 22 MHz, with major structures.

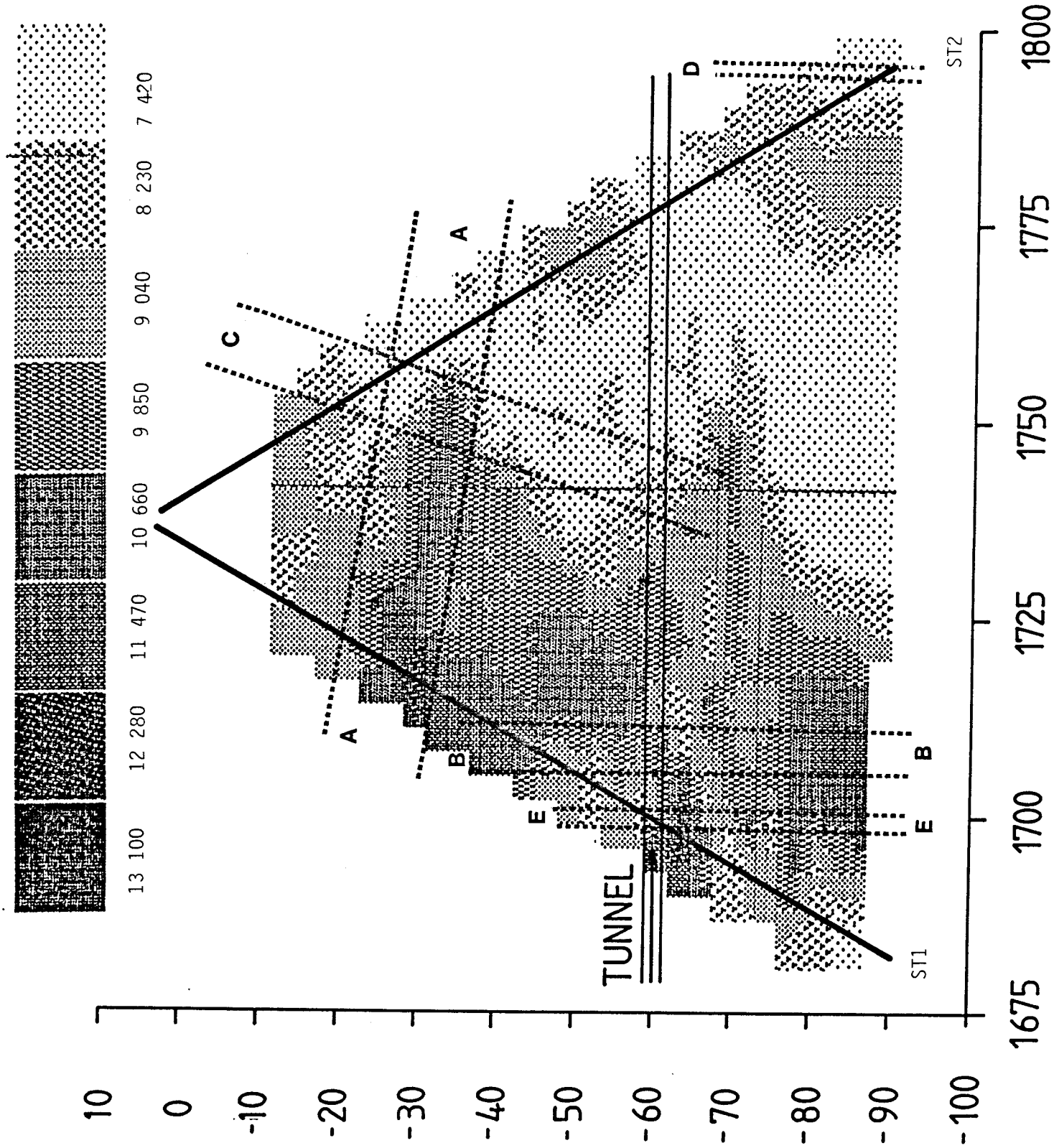

Figure 4.12 Radar tomogram showing the distribution of slowness in the plane between the boreholes obtained at the crosshole measurements between ST1 and ST2 at a center frequency of 22 MHz, with major structures.

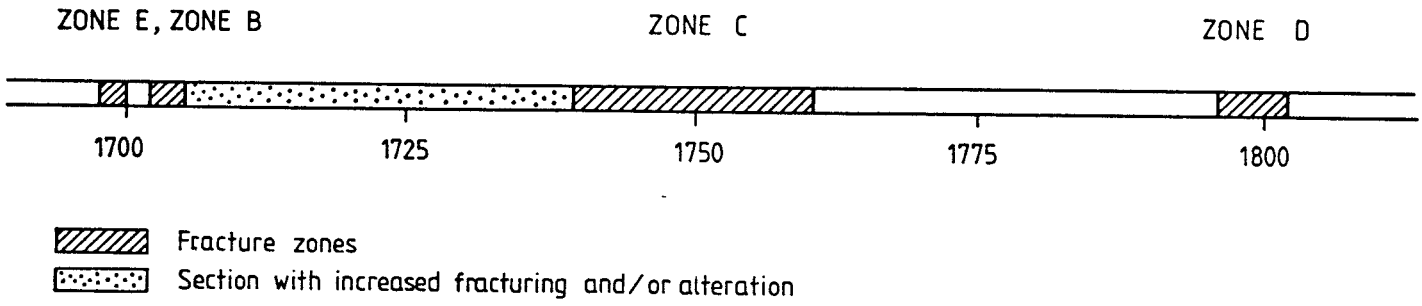

Figure 4.13 Tunnel with calculated intersections of radar interpreted structures.

5 COMBINED INTERPRETATION

5.1 Major structures interpreted by borehole radar measurements compared to geological, geophysical and hydraulic results.

The radar model of the main structures indicated a set intersecting the site with a steep dip and striking NNW. Observe that all directions in this and the following chapters are given with reference to geographical north. A semi-horizontal structure which intersects the boreholes at a vertical depth of about 30 m has also been identified. Four structures with steep dip are interpreted from the tomograms, see Figs 4.11 and 4.12. The attenuation of the radar waves at the investigated site is high which is an indication of relatively intense fracturing and/or alteration. The high attenuation at the site is also caused by the complex lithology which contains several contacts between different rock types.

The following is a comparison of radar interpreted major structures to the results of the geological core mapping, the geophysical logging and the hydraulic tests. The different logs are displayed in Figs. 5.1 and 5.2.

Structure A (ST1: 28-41 m, ST2: 34-49 m).

The existence and strike of the structure is confirmed by all available investigation methods. The interpretation of the crosshole radar measurements shows that the structure can be correlated between the boreholes as a subhorizontal structure. The depth in ST1 (G2/P2: 32-39 m) and ST2 (G4/P7+P8: 41-50 m) has been determined on the basis of geophysical logging and geological core mapping. The structure is the most dominating of all encountered structures in the investigated area.

Zone B (ST1: 50-63 m).

The position of B is uncertain due to the difference between the amplitude and traveltime tomograms. The position and strike of this structure in ST1 can not be verified exactly from the geophysical

logging or geological core mapping. However, the lower part of structure B coincides with P3 (61-68 m).

Structure C (ST2: 25-35 m).

This structure can not directly be verified as a fracture zone from geophysical logging results or geological core mapping in ST2. However,the upper section of the structure, interpreted from tomography, overlap a geophysically interpreted section (P6: 21-26 m) and the structure can be referred to lithological variations. The singlehole radar shows that a reflection agrees with the geophysically interpreted contact between granite and migmatite (P6). The fact that lithological boundaries in some cases are accompanied by radar reflections is probably the explanation of the irregular behaviour of the corresponding structures in the crosshole measurements.

Structure C, as seen from the radar measurements and which probably can be referred to as a lithological boundary, do not exhibit a straight planar shape in the tomograms but is interpreted to be more or less vertical with a strike roughly N-S. This implies that the lithology within the investigated area should have the same orientation.

Structure D (ST2: 107-109 m).

The geophysical logging was performed down to 107 m in ST2 and did not reach the depth of the interpreted structure. Geological core mapping shows a somewhat higher fracture frequency and a lithological contact at the actual intersection. The structure is not considered to be prominent. The structure is interpreted to be vertical and have a strike roughly N-S which is more or less parallel to structure C. Location inferred from amplitude tomogram is slightly displaced in travel time tomogram. Errors in tomograms towards the end of the borehole can be due to poor ray coverage.

Structure E (ST1: 73-75 m).

The intersection of the structure with ST1 is verified both by geological core mapping by a somewhat higher fracture frequency and geophysical logging. However, the orientation of the structure can not be clearly deduced from the available geological or geophysical logging data.

5.2 Geophysical, geological and hydraulic data compared with radar interpreted structures.

The interpreted zones, discussed below, follows the geophysical and geological criteria for determination of fractures/fracture zones, defined in chapters 4.1 and 4.2, and listed in Table 4.1. Numbered zones with prefix P refers to geophysical logging and prefix G to geological mapping.

Borehole ST1

Zone G1/P1 (5-8 m)

From the geological core mapping this is a clearly observed fracture zone, characterized by >10 fractures/m, mylonitization, tectonization, red colouring and alteration. The geophysical logging resulted in anomalies following the criteria for fracture zones put up in chapter 4.2. The hydraulic conductivity is relatively high, confirming the interpretation of a permeable fracture zone. This G1/P1 zone is also detected by singlehole radar reflections at 7 m, showing an angle of 30^{o} to the borehole axis (22 and 60 MHz). This zone is interpreted to be the same zone as G3/P5 in ST2, a parallel zone to the deeper positioned structure A from the tomograms. In the combined interpretation it has been denominated zone I.

Zone G2/P2 (32-39 m)

From the geological core mapping this section is interpreted as a fracture zone. The zone is characterized by >10 fractures/m,

mylonitization, crushed sections, red colouring, alteration and contacts between different rock types. From geophysical logs this section is interpreted as a fracture zone by having a marked low resistivity and high neutron ratio. Also, the zone has a high hydraulic conductivity, as seen from the singlehole hydraulic tests.

The G2/P2 zone is detected by the singlehole radar measurements and the reflections indicate a NW strike and a 35^{o} dip towards NE. The tomograms exhibit a structure (A) which covers the G2/P2 zone and is interpreted to be the same zone. The G2/P2 zone is interpreted to be the same as G4/P7+P8 in ST2. In the combined interpretation it has been denominated zone II.

Zone P3 (61-68 m)

This zone is, from the geophysical logging,interpreted as a lithological structure with an increased fracture frequency. The core mapping shows a somewhat higher fracture frequency where also infillings of calcite and/or quartz can be observed. The mapped fractures intersects the borehole 35^{o} to the borehole axis.

The singlehole radar measurement also detects and confirms the fractures within this section. At 62 m, the detected reflections indicate an intersection to the borehole with 30^{o} and 15^{o}, for 22 MHz and 60 MHz, respectively. The strike of this zone is N-S with a vertical dip. The zone is represented by the lower part of radar structure B in the tomograms.

Zone P4 (75-78 m)

This low-resistive zone, as detected by the logging, is interpreted as a fracture zone. The core mapping shows a somewhat higher fracture frequency and several healed fractures with calcite. Also, the hydraulic conductivity is slightly higher than the average for the borehole.

Reflections from the singlehole radar measurement that could be directly related to this zone can not observed. However, there is a

reflection which indicates an intersection of a structure in the borehole at 72 meter with an angle of 50^{o} to the borehole (22 MHz). The position in the tomograms is represented by radar structure E which was interpreted as vertical in the radar model. The orientation of the zone is by the combined interpretation considered to be parallell to both the G1/P1-G3/P3 zone and structure A. The changed orientation is also possible to interpret from the tomograms.

Zone P4 is interpreted to be parallell to radar structure A and intersecting ST2 in section G6/P11, thereby having an orientation of NW/35 NE. In the combined interpretation it has been denominated zone III.

Borehole ST2

Zone G3/P5 (5-8 m)

From the geological core mapping this section is interpreted as a fracture zone. The zone is characterized by >10 fractures/m, mylonitization, tectonization, red colouring and alteration. The geophysical logging also recorded this section as a fracture zone, by having low resistivity and high neutron ratio. No suitable radar reflections can be observed. The zone is interpreted to be the same zone as G1/P1 in ST1, parallell to the deeper positioned structure A from the tomograms. In the combined interpretation it has been denominated zone I.

Zone P6 (21-26 m)

The geophysical logging recorded this section as a low resistive zone which would indicate fractures/fracture zone. But, the core mapping revealed few fractures within this section. As a consequence, this low resistive zone is interpreted as a result of lithological variations. The singlehole radar shows one reflection at 25 m with an angle of 35^{o} (22 MHz) which is interpreted to be caused by lithological contacts. The section overlaps the radar interpreted structure C. The strike is N-S and the dip is vertical.

Zone G4/P7+P8 (41-50 m)

This is a clearly observed fracture zone interpreted to be the same zone as G2/P2 in ST1 and radar structure A from the tomograms. This zone is characterized in the same way as G2/P2, but with the difference that the geophysical logging and core mapping reveal that the zone consists of two separate smaller parts. Singlehole radar reflections occur at 39 m and 47 m with angles 40^{o} and 35^{o}. The strike is NW and the dip is 35^{o} towards NE. In the combined interpretation it has been denominated zone II.

Zone P9 (53-55 m)

This zone is, from the geophysical logging, interpreted as a 2 meter wide fracture zone, correlated to a lithological contact, interpreted from the logging results, at 55 metres depth. The zone is, from the core mapping, characterized by a somewhat higher fracture frequency and red colouring. The zone is relatively subordinate. Singlehole radar reflections occur at 56 m with 15^{o} and 18^{o}, respectively (60 MHz). The strike is N-S and the dip is vertical.

Zone G5/P10 (68-71 m)

This 3 meter section is interpreted as a fracture zone correlated to a lithological contact at 71 metres depth. This contact between granite and migmatite is also detected by the singlehole radar measurements. The intersection of the zone is interpreted, from the radar, to 71 metres depth with an angle of 21^{o} (60 MHz). The strike is N-S and the dip is vertical.

Zone G6/P11 (80-83 m)

From the geophysical logging and the core mapping, this section is interpreted as a fracture zone. The zone is characterized by >10 fractures/m, red colouring, alteration and a relatively low resistivity. The hydraulic conductivity is higher in this zone,

confirming the fracture zone.

This zone (80-83 m) is interpreted to be the same zone as P4 detected in ST1. The hydraulic conductivity for the zone measured in ST2 is higher than the corresponding section in ST1. This can be due to the occurence of chlorite and absence of calcite in this section in ST2. There is also a singlehole radar reflection at 80 m with an angle of 23^{o} (60 MHz) to the borehole axis. In the combined interpretation it has been denominated zone III.

5.3 Results of combined interpretation.

From the combined interpretation it seems clear that at least two sets of main structures in the rock mass exist at the investigation site. One set is striking roughly N-S with a dip more or less vertical and the other is directed to NW with a dip of about 35^{o} towards NE, i.e. a subhorizontal set. The vertical structures seem to be coupled to lithological variations in the rock, such as rock contacts between different combinations of migmatite, granite and pegmatite. These rock contacts are often accompanied by a somewhat higher fracture frequency. The geophysical logging also supports this interpretation. However, the hydraulic conductivity is in general not very high in connection to these structures. Most of the singlehole radar reflections seem to be correlated to these lithological contacts. Altogether, it can be assumed that the vertical set is not very prominent in the rock mass at the site and is associated with lithology. The other set is connected to a high degree of tectonization and fracturing. In this set lithological variations seem to play a minor role. The sections representing this set in the boreholes exhibit the largest geophysical anomalies encountered in the holes. Also, the hydraulic conductivity in these sections is the highest encountered in the boreholes. The singlehole radar reflections representing this set of fractures are rather weak. Except for the high attenuation at the site, the poor radar response can also be caused by the large angle of the set relative borehole axis which is unfavourable for obtaining radar reflections. However, the tomograms in return show the two interpreted subhorizontal zones II and III (structure A and E in the tomograms) although with a displacement downwards of about 10 m.

Altogether the combined model of the site can be described by the following:

* A set of features with lithologic origin striking roughly N-S and having a vertical dip. These features are not prominent and are thereby considered to play a minor role in the area.

* Zone I (G1/P1-G3/P5) which is mainly interpreted from the geological core mapping and geophysical logging as a rather prominent semi-horizontal fracture zone with tectonization and high hydraulic conductivity. The zone is parallel to zone II and III.

* Zone II (Structure A and G2/P2-G4/P7+8) which is the most prominent zone encountered in the area. The zone is interpreted from radar, geological mapping, geophysical logging and hydraulic measurements as a semi-horizontal zone, parallel to zone I and III.

* Zone III (Structure E and P4-G6/P11) which is interpreted from radar, geological mapping, geophysical logging and hydraulic conductivity as a semi-horizontal zone, parallel to zone I and II.

Figs. 5.3 and 5.4 show the result from the combined interpretation. The zones with orientation and intersection in boreholes and tunnel are listed in Table 5.1. In Table 5.2 is a comparison of the interpreted zones made in order to show the very good agreement between the zones interpreted from the respective methods, used within this study. When this table is compared to Tables 4.5 - 4.8 it can be seen that the radar generally shows more reflectors than there are interpreted major zones, i.e. the radar is also sensible for structures with lithological origin as well as fracture zones.

Table 5.1 Orientation and intersection in boreholes and tunnel of the major zones from the combined interpretation. Strike is given in geographical north and coordinates are given in the local grid.

Zone	Orientation	ST1	ST2	Tunnel
I	Semi-horizontal	5-8 m	5-8 m	Parallel
II	NW/35 NE	32-39 m	41-50 m	1860-1910
III	NW/35 NE	75-78 m	80-83 m	1620-1690

Table 5.2 Comparison of position of interpreted zones from the different investigations.

Depth (m)	Combin. interp.	Radar invest.	Geological core mapping	Geophysical logging	High hydraulic conductivity (m)
ST1					
5-8	I	*	G1	P1	5-15
32-39	II	A	G2	P2	29-31,33-35
50-63		B	-	-	45-65
61-68		*	-	P3	
75-78	III	E	-	P4	77-81
ST2					
5-8	I	-	G3	P5	5-15
25-35		C	-	P6	
41-50	II	A	G4	P7+P8	41-43,43-45
53-55		*	-	P9	
69-71		*	G5	P10	71-73
80-83	III	E	G6	P11	81-83

* = Singlehole radar reflection

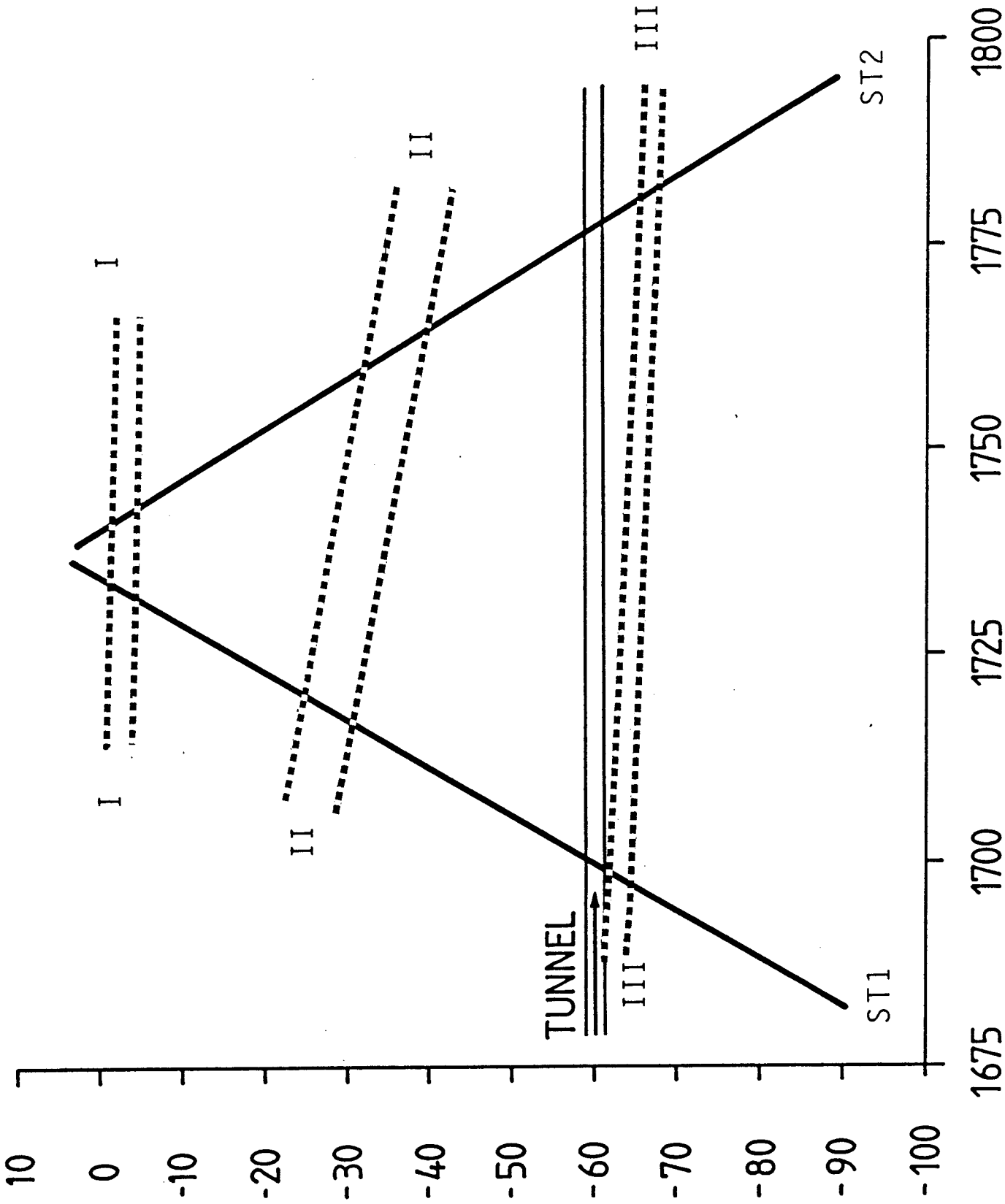

Figure 5.3 Major zones in the boreholes ST1 and ST2 at the Saltsjötunnel, interpreted from the combined results.

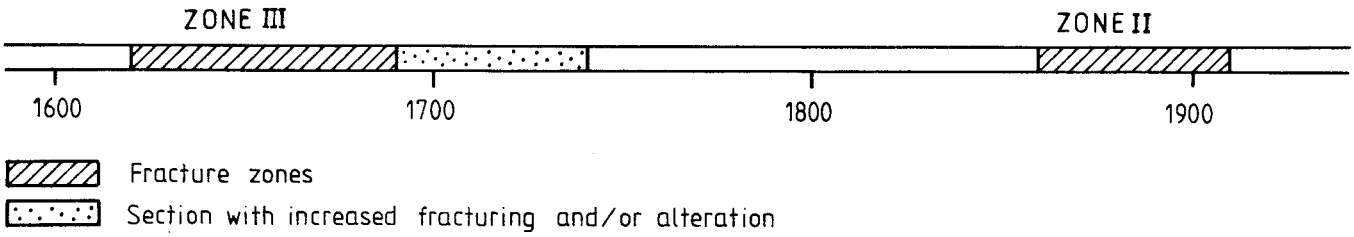

Figure 5.4 Major zones in the Saltsjötunnel, interpreted from the combined results.

6 CONCLUSIONS

The geological model produced by the radar results have in general been confirmed by all other available data recorded during this project. The combined interpretation reveals two different sets of fractures within the rock mass.

The radar results from the Saltsjötunnel site have demonstrated the capability of the radar method to identify and describe the geometry of geologic structures at a distance of up to 50 m from the boreholes. The definition of the geometry has in this case not been as good as is theoretically possible due to drift problems with the equipment. When the radar results have been compared to results from standard borehole investigations such as core mapping, singlehole geophysical logging, and hydraulic tests it has been possible to give the radar features a geologic description. The features have also been described with respect to their physical and hydraulic properties. The majority of features observed in the singlehole radar measurements appear to be associated with lithologic boundaries and the increase in fracturing in connection to these boundaries. The features found in the radar tomograms are caused by a set of subhorizontal fracture zones with significant tectonization and large hydraulic conductivities.

High hydraulic conductivity has not been observed outside the interpreted zones and structures, except for one case in ST2.

The agreement between geologically and geophysically interpreted zones is very good.

Three major zones have been interpreted from the combined investigations, all of them subhorizontal. The major zones are interpreted as fracture zones. One set of vertical features originating from lithological structures have also been interpreted from the combined investigations.

7 DISCUSSION

The fact that the large number of lithological boundaries, within the site, are accompanied by radar reflections explains the high attenuation of radar waves in the area, thus causing the radar probing range to be low compared to most other investigated areas (about 30 metres in singlehole mode). The high attenuation generally causes the radar reflections to be weak and sometimes difficult to interpret. The high attenuation and the heterogeneous rock mass is probably the explanation to the irregular behaviour of the structures observed in the crosshole measurements.

From the radar results four, nearly vertical, structures (B, C, D and E) were interpreted to be correlated to the first set of features, i.e. associated with lithological variations. These nearly vertical features are in general verified by geophysical logging and geological core mapping. However, structure E was in the combined interpretation assumed to consist of two different sets of features; one vertical which is associated with lithology as already pointed out from the radar model and one subhorizontal which was interpreted as zone III. This horizontal zone III is parallell to and characterized in the same way as zone II and intersects boreholes ST1 and ST2. The position of zone III in the borehole ST1 is also indicated in the tomograms, although with a displacement of about 10 metres and interpreted as a vertical zone.

Structure B as defined in the radar model cannot be directly verified by means of the other available data. However, results from both the geophysical logging and the geological core mapping indicates lithological variations within this section (rock contacts and minor fractures) which can be the origin of the radar response.

The horizontal zone II in the combined model, was defined by the radar model and is clearly verified by all other data. This zone is the most dominating of all encountered zones in the area. The tomograms are indicating a position of zone II, some metres deeper than the position determined by geophysical logging and geological core mapping. The final depth position of zone II is interpreted from the logging and core mapping.

Furthermore, the combined interpretation revealed two fracture zones, parallell to zone II, situated on both sides of II. The deepest positioned, of these three nearly horizontal zones is the one referred above (zone III) and intersecting the boreholes ST1 and ST2 in sections P4/E and G6/P11, respectively. The combined interpretation also indicates a zone I, parallell to II, close to the ground surface and intersecting ST1 and ST2 in sections G1/P1 and G3/P5, respectively. The character of this zone is identical to the horizontal zones observed deeper down in the boreholes.

The singlehole radar response from these three horizontal zones are in general weak. The only exception is zone II which gave distinct radar response. The probable explanation of the small radar response, from the horizontal zones, is the high radar attenuation in combination with the large angle between the borehole axis and the zones, which is unfavourable for obtaining radar response.

The three subhorizontal zones are interpreted to be the most dominating fracture zones within the investigated area. This is clearly confirmed by the high hydraulic conductivity as measured during the singlehole hydraulic tests.

In Fig. 5.3 is the major zones, interpreted from the combined results visualized. A view of the tunnel with the interpreted major zones are presented in Fig. 5.4, the figure also shows the section interpreted from the tomograms with low velocity and high attenuation.

One problem in the interpretation of the radar data was the difference in intersection angles observed between the 22 MHz and the 60 MHz measurements. There is a systematic difference where the 60 MHz angles are generally smaller. This difference was caused by a temperature drift in the time base of the radar system. The radar system has now been modified and errors of this type should not occur in future measurements. The temperature drift has caused a systematic error in the intersection angles. Attempts have been made to correct for the drift but it has not been possible to find a reliable way to determine the magnitude of the correction.

The errors in the intersection angles have caused a considerable

uncertainty in the interpretation of the singlehole reflection measurements. However, it is found that the intersection angles obtained in the two holes are roughly the same. This gives two possible orientations for the structures causing the majority of the radar reflections: a strike roughly N-S and steep dip or a strike E-W with a dip of 40 to 50 degrees. When the radar results have been compared to the other borehole data it was found that most radar reflectors are associated with lithological contacts striking roughly N-S. There are also a few radar reflectors which are associated with a set of subhorizontal fracture zones which strike NW and dip 35 degrees to NE. This second set is seen more clearly in the tomograms.

Another interesting aspect of the tomograms is the difference in attenuation and velocity between the western and eastern parts of the plane between the boreholes. The attenuation is higher and velocity is lower in the western part indicating that the rock in this region is more fractured or has a more heterogeneous lithology than the eastern part. There is no clear indication of the cause for this difference in the borehole data and the cause for this difference will have to be checked by observations in the tunnel.

REFERENCES

Almén, K.-E., Hansson, K., Johansson, B.-E., Nilsson, G., Andersson, O., Wikberg, P., and Åhagen, H., 1983. Final disposal of spent nuclear fuel - equipment for site characterization. KBS TR 83-44. SKBF/KBS, Stockholm, Sweden.

Almén, K.-E., Andersson, O., Fridh, B., Johansson, B.-E., Sehlstedt, M., Gustafsson, E., Hansson, K., Olsson, O., Nilsson, G., Axelsen, K., and Wikberg, P., 1986. Site investigation - Equipment for geological, geophysical, hydrogeological and hydrochemical characterization. SKB TR 86-16. SKB, Stockholm, Sweden.

Andersson, J-E., 1987. Interpretation of single-hole hydraulic tests in the boreholes ST1 and ST2 at the Saltsjötunnel. SKB AR 87-10. SKB, Stockholm, Sweden.

Carlsten, S. and Magnusson, K.-Å., 1985. Crosshole investigations - Description of the small scale site. Stripa project IR 85-05. SKB, Stockholm, Sweden.

Carlsten, S., Falk, L., Olsson, O., 1987. Interpretation of radar measurements in the boreholes ST1 and ST2 at the Saltsjötunnel. SKB AR 87-11. SKB, Stockholm, Sweden.

Ivansson, S., 1984. Crosshole investigations - Tomography and its application to crosshole seismic measurements. Stripa Project, IR 84-08, SKB, Stockholm, Sweden.

Olsson, O., Sandberg, E., Nilsson, B., 1983. The use of Borehole radar for the detection of fractures in crystalline rock. Stripa Project, IR 83-06, SKBF/KBS, Stockholm, Sweden.

Olsson, O., Sandberg, E., 1984. Preliminary design of a new borehole radar system. Stripa Project, IR 84-04, SKBF/KBS, Stockholm, Sweden.

Olsson, O., Falk, L., Forslund, O., Lundmark, L., Sandberg, E., 1987. Crosshole investigations - Results from borehole radar investigations. Stripa Project, (in print). SKB, Stockholm, Sweden.

Schlumberger, 1972. Log interpretation, volume 1 - Principles. Schlumberger Ltd., USA.

Serra, O., 1984. Fundamentals of well-log interpretation: 1. The aquisition of data. Elsevier science publishers b.v. Netherlands, ISBN 0-444-42132-7.

Stråhle, A., Stejskal, V., 1987. Rock and fracture logging, the Saltsjötunnel boreholes ST1 and ST2. SKB AR 87-09. SKB, Stockholm, Sweden.

Stålhös, G., 1969. Beskrivning till Stockholmstraktens berggrund (Description to geological map sheet of Stockholm with surroundings). Swedish Geological Survey, Ser.: Ba 24. Stockholm, Sweden. (In Swedish with English summary).

APPENDIX 1

Technical data for boreholes ST1 and ST2 at the Saltsjötunnel. Coordinates are given in the local grid.

		ST1	ST2
Declination	(Gons)	205	399
	(Deg.)	184.5	359
Inclination	(Gons)	66	65
	(Deg.)	59.4	58.5
Position	X (m)	1736.26	1738.2
	Y (m)	-0.06	0.09
	Z (m)	3.34	3.46
Length	(m)	110	110

List of SKB reports

Annual Reports

1977–78
TR 121
KBS Technical Reports 1 – 120.
Summaries. Stockholm, May 1979.

1979
TR 79–28
The KBS Annual Report 1979.
KBS Technical Reports 79-01 – 79-27.
Summaries. Stockholm, March 1980.

1980
TR 80–26
The KBS Annual Report 1980.
KBS Technical Reports 80-01 – 80-25.
Summaries. Stockholm, March 1981.

1981
TR 81–17
The KBS Annual Report 1981.
KBS Technical Reports 81-01 – 81-16.
Summaries. Stockholm, April 1982.

1982
TR 82–28
The KBS Annual Report 1982.
KBS Technical Reports 82-01 – 82-27.
Summaries. Stockholm, July 1983.

1983
TR 83–77
The KBS Annual Report 1983.
KBS Technical Reports 83-01 – 83-76
Summaries. Stockholm, June 1984.

1984
TR 85–01
Annual Research and Development Report 1984
Including Summaries of Technical Reports Issued during 1984. (Technical Reports 84-01– 84-19)
Stockholm June 1985.

1985
TR 85-20
Annual Research and Development Report 1985
Including Summaries of Technical Reports Issued during 1985. (Technical Reports 85-01-85-19)
Stockholm May 1986.

1986
TR86-31
SKB Annual Report 1986
Including Summaries of Technical Reports Issued during 1986
Stockholm, May 1987

Technical Reports

1987

TR 87-01
Radar measurements performed at the Klipperås study site
Seje Carlsten, Olle Olsson, Stefan Sehlstedt, Leif Stenberg
Swedish Geological Co, Uppsala/Luleå
February 1987

TR 87-02
Fuel rod D07/B15 from Ringhals 2 PWR: Source material for corrosion/leach tests in groundwater
Fuel rod/pellet characterization program part one
Roy Forsyth
Studsvik Energiteknik AB, Nyköping
March 1987

TR 87-03
Calculations on HYDROCOIN level 1 using the GWHRT flow model
Case 1 Transient flow of water from a borehole penetrating a confined aquifer
Case 3 Saturated-unsaturated flow through a layered sequence of sedimentary rocks
Case 4 Transient thermal convection in a saturated medium
Roger Thunvik, Royal Institute of Technology, Stockholm
March 1987

TR 87-04
Calculations on HYDROCOIN level 2, case 1 using the GWHRT flow model
Thermal convection and conduction around a field heat transfer experiment
Roger Thunvik
Royal Institute of Technology, Stockholm
March 1987

TR 87-05
Applications of stochastic models to solute transport in fractured rocks
Lynn W Gelhar
Massachusetts Institute of Technology
January 1987

TR 87-06
Some properties of a channeling model of fracture flow
Y W Tsang, C F Tsang, I Neretnieks
Royal Institute of Technology, Stockholm
December 1986

TR 87-07
Deep groundwater chemistry
Peter Wikberg, Karin Axelsen, Folke Fredlund
Royal Institute of Technology, Stockholm
June 1987

TR 87-08
An approach for evaluating the general and localized corrosion of carbon steel containers for nuclear waste disposal
GP March, KJ Taylor, SM Sharland, PW Tasker
Harwell Laboratory, Oxfordshire
June 1987

TR 87-09
Piping and erosion phenomena in soft clay gels
Roland Pusch, Mikael Erlström,
Lennart Börgesson
Swedish Geological Co, Lund
May 1987

TR 87-10
Outline of models of water and gas flow through smectite clay buffers
Roland Pusch, Harald Hökmark,
Lennart Börgesson
Swedish Geological Co, Lund
June 1987

TR 87-11
Modelling of crustal rock mechanics for radioactive waste storage in Fennoscandia—Problem definition
Ove Stephansson
University of Luleå
May 1987

TR 87-12
Study of groundwater colloids and their ability to transport radionuclides
Kåre Tjus* and Peter Wikberg**
*Institute for Surface Chemistry, Stockholm
**Royal Institute of Technology, Inorganic Chemistry Stockholm
March 1987

TR 87-13
Shallow reflection seismic investigation of fracture zones in the Finnsjö area method evaluation
Trine Dahl-Jensen
Jonas Lindgren
University of Uppsala, Department of Geophysics
June 1987

DEPTH (m)

LITHOLOGY
- Geological mapping
- Geophysical logging

FRACTURES
- Mapped fracture frequency (frac/m) — 10, 20
- Geophysical interpreted fractures

RQD — 50, 100

INTERPRETED ZONES
- Geological mapping: G1, G2, P3, P4
- Geophysical logging: P1, P2

TRANS-MISSIVITY (m^2/s) — 10^{-8}, 10^{-6}, 10^{-4}

INTERPRETED RADAR STRUCTURES
- CROSS-HOLE
- SINGLEHOLE 22MH: A, B, E
- SINGLEHOLE 60 MHz

GRANITE MIGMATITE PEGMATITE
NOT DEFINABLE
FRACTURED
HIGHLY FRACTURED
10 M
2 M

Figure 5.1 Results from the combined investigations in ST1 at the Saltsjötunnel.

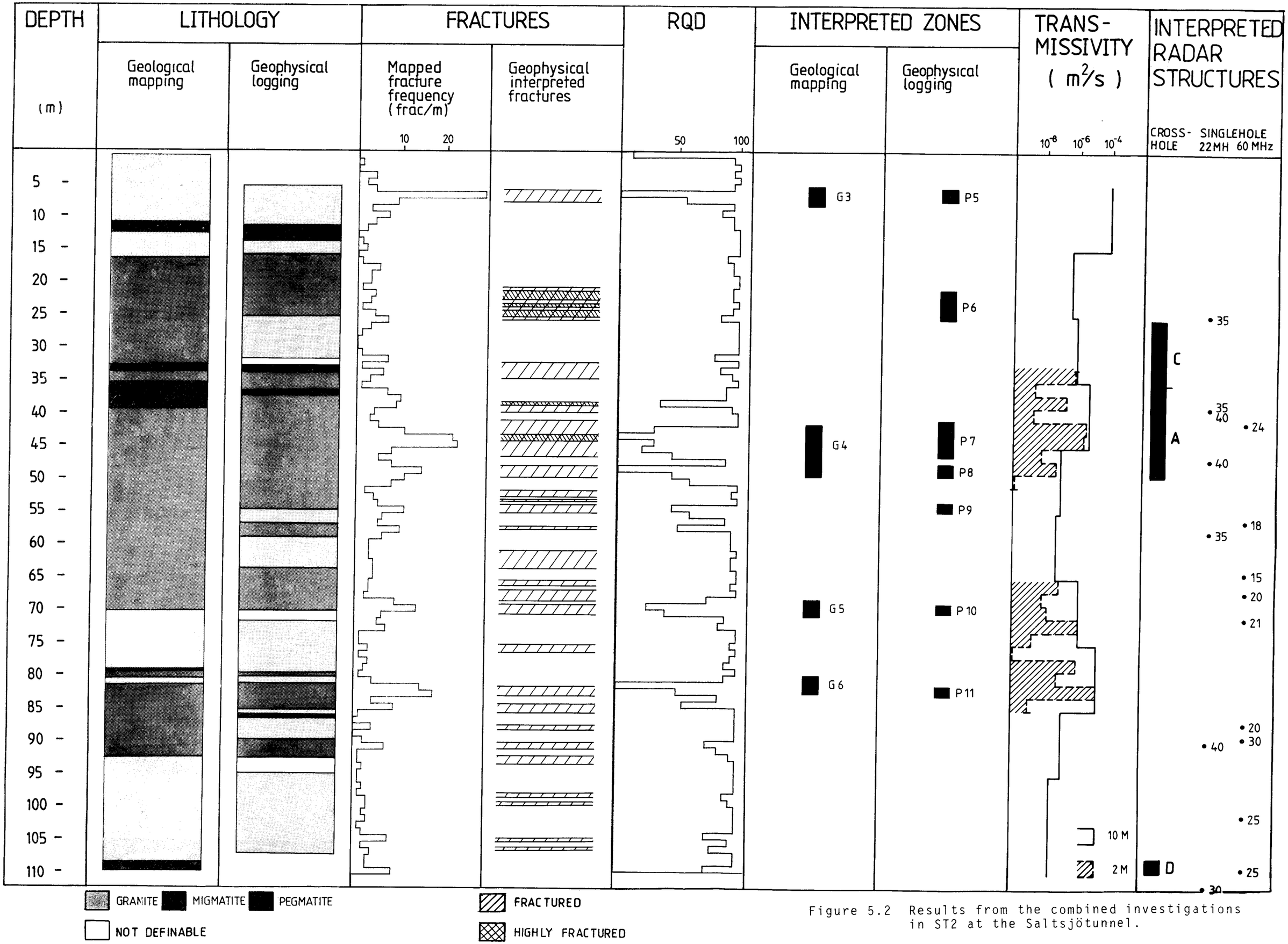

Figure 5.2 Results from the combined investigations in ST2 at the Saltsjötunnel.